AEDC-TDR-62-172

AN ANALYSIS OF NONEQUILIBRIUM INVISCID FLOWS

By

W. E. Gibson and A. Sowyrda

Cornell Aeronautical Laboratory, Inc.

Buffalo, New York

(The reproducible copy supplied by the authors was used in the reproduction of this report.)

August 1962

FOREWORD

The research work on which this report is based was performed by Dr. W. E. Gibson and Mr. A. Sowyrda of the Aerodynamic Research Department of Cornell Aeronautical Laboratory, Inc., Buffalo, New York, under Air Force Contract No. AF 40(600)-928. The Arnold Engineering Development Center, Air Force Systems Command, was the monitoring agency.

ABSTRACT

An analytic solution is developed for blunt-body flows involving nonequilibrium chemistry. The chemical model describes a diatomic gas with a single dissociation recombination reaction. The progress of the reaction is determined behind the bow shock under conditions of vibrational equilibrium. The analysis seeks an improved understanding of the structure of the chemical relaxation zone along streamlines, in particular, its dependence on flow parameters.

In high-altitude flight, three-body recombination becomes ineffective[1] and dissociation or binary scaling can be applied. The range of validity of binary scaling is found and the implications for hypersonic testing are discussed. The analytic approach also applies for cases where recombination is important, including equilibrium flow. Numerical examples are given for spherical bodies and for a range of body sizes and flight altitudes.

TABLE OF CONTENTS

TABLE OF CONTENTS (CONT.)

LIST OF SYMBOLS

a	defined in Eqs. (34)
A	defined in Eq. (28)
$\bar{A}$	pressure gradient given in Eq. (56)
b	defined in Eqs. (34)
$\bar{b}$	defined in Eqs. (58)
C	rate coefficient for Lighthill gas; cf. Eq. (20)
$\bar{C}$	equal to $C T_d^{-s}$
E	total energy of a blast wave
$F(\alpha, T', \rho', \eta)$	normal shock function for a Lighthill gas; cf. Eq. (22)
h	dimensionless enthalpy = $\frac{i}{v_d^2}$
h_∞	dimensionless enthalpy of the free stream = $\frac{1}{2} M_d^2$
i	internal enthalpy
$I(\alpha; h)$	dissociation integral defined in Eq. (25)
k	nose drag coefficient
k_F	forward rate coefficient
k_R	reverse rate coefficient
L	length scale for steady flow
L^*	length scale for a blast wave
M_d	Mach number based on v_d ; cf. Eq. (5)
M_d'	Mach number based on $\frac{v_d}{b}$; cf. Eq. (9)

LIST OF SYMBOLS (CONT.)

$\mathcal{M}$	molecular weight of Lighthill gas
p	gas pressure
p_d	dissociation pressure = $R_o \rho_d T_d$
p'	dimensionless pressure = $\frac{p}{\rho_\infty U_\infty^2}$
q	gas velocity
q'	dimensionless velocity = $\frac{q}{U_\infty}$
R_F	forward rate of chemical generation
R_N	nose radius in Eq. (6)
R_R	reverse rate of chemical generation
R_s	shock radius
$\mathcal{R}$	universal gas constant
R_o	gas constant per mole = $\frac{\mathcal{R}}{\mathcal{M}}$
R_1	ratio of recombination to dissociation rate; $\frac{\alpha^2}{1-\alpha} \eta \rho' \exp \frac{1}{T'}$ for Lighthill gas
s	temperature exponent of recombination rate; cf. Eq. (20)
S'	dimensionless entropy function; cf. Eq. (14)
t^*	time scale for a nonequilibrium blast-wave; defined on p. 13
T	gas temperature
T_d	dissociation temperature = 6×10^4°K for O_2
T'	dimensionless temperature = $\frac{T}{T_d}$

LIST OF SYMBOLS (CONT.)

T_o'	dimensionless temperature at the turning point; defined by Eq. (40)
u	gas velocity in a normal shock
U_∞	velocity of the free stream
v_d	reference velocity = $\sqrt{R_o T_d}$
V'	denotes dimensionless functions in Eqs. (8), (11) and (12)
α	degree of dissociation for a Lighthill gas
(α)	chemical concentrations for a complex system
α_f	frozen concentrations in afterbody flow; cf. Eq. (13)
α_o	concentration at the turning point; defined by Eq. (40)
$\bar{\alpha}$	defined in Eqs. (47)
β_o	equal to recombination rate at turning point, $\nu_R(\zeta_o)$, cf. Eq. (43)
γ_f	adiabatic exponent for frozen afterbody flow; cf. Eq. (15)
γ_s	adiabatic exponent at the shock; defined in Eqs. (1)
γ'	equivalent adiabatic exponent for equilibrium flow; given by Eq. (35)
δ	standoff distance
δ_o	defined in Eqs. (51)
$\bar{\delta}_o$	defined in Eqs. (58)
ϵ	small parameter of Newtonian theory; $\frac{1}{\epsilon} = \frac{\rho_s}{\rho_\infty}$
ζ	streamline coordinate; defined by Eqs. (36) and (37)
ζ_{max}	defined in Eq. (38)

LIST OF SYMBOLS (CONT.)

ζ'_{max}	defined in Eq. (64)
$\bar{\zeta}$	defined in Eq. (47)
ζ_o	value of ζ at the turning point
η	altitude parameter; defined in Eq. (7)
η_o	a given value of η ; cf. Section 2.1
ξ	angular coordinate defined in Section 3.1
ϑ_{max}	maximum value of ϑ for which $\zeta = \zeta_{max}$; cf. Section 3.3
Θ_s	angle of the shock with the free stream; cf. Eqs. (1)
$\varkappa$	variable for normal shock solution in a Lighthill gas; defined in Eq. (21)
$\varkappa_{rec}$, $\varkappa_{a\,rec}$	value of $\varkappa$ at the scaling limit; see Section 2.1
ψ	stream function
Λ	scaling parameter for nonequilibrium flows; defined in Eq. (6)
Λ^*	scaling parameter for a blast wave; defined in Eq. (17)
$\bar{\Lambda}$	defined in Eq. (31)
$\bar{\Lambda}_1(h)$	value of $\bar{\Lambda}$ such that $T'_o = T'_s = \frac{h}{4}$; cf. Section 3.4
$\bar{\Lambda}_2(h,\eta)$	value of $\bar{\Lambda}$ such that $T'_o = T'_{e,s}$; cf. Section 3.4
μ_o	coefficient defined in Eq. (46)
ν	equal to zero for two-dimensional flow; equal to one for axisymmetric flow

INTRODUCTION

Real-gas effects play an ever increasing role in research pertaining to hypersonic flight through planetary atmospheres. They are established in a complex interaction between chemical processes in high-temperature gases and fluid-dynamic expansions. Technically important examples are given by nozzle flows and hypersonic flows about blunted bodies Recent theoretical work in these areas has a dual objective: prediction of real-gas effects in flight situations and correlation of flight tests with laboratory experiments. Exact numerical solutions are now available[2] for both nozzle flows and blunt-body flows with the coupled nonequilibrium chemistry of high-temperature air. Concurrently, there exists a pressing need for analytic approximations which stress the basic features of seemingly different solutions. For instance, analytic solutions should clarify the dependence of real-gas effects on flow parameters and suggest scaling laws which would be of paramount importance in the interpretation of experimental data.

Analytic methods were first represented by linearized theories[3, 4] which assume small departures from an initial state of chemical equilibrium in flow past an airfoil. The work of Refs. 3 and 4 typifies this approach. The transition to a new level of chemical equilibrium appropriate to the airfoil shape occurs through diffusion of Mach waves. The leading wave proceeds with a sound speed corresponding to frozen

chemistry; eventually, the main part of the disturbance is shifted to an equilibrium wave. Using the closeness of frozen to equilibrium speed of sound, one is able to describe the transition by solving a simple telegraph equation.[3] The existence of two sound speeds is a basic feature of nonequilibrium flows and the above studies should help to establish characteristic methods for supersonic, nonequilibrium flows.

Another basic trait is the variation of relaxation time with temperature. This effect is responsible for chemical freezing in rapid flow expansions, as strikingly demonstrated by nozzle flow solutions.[2] Here, a nonlinear analytic theory is required. The present report develops such a theory for the case of blunt-body flows. The approach is based on the Newtonian assumptions made in Ref. 5 which are most accurate for the high compressions associated with hypersonic nonequilibrium flows. Then, Newtonian theory provides simple solutions for velocity and pressure distributions which are, in the first approximation, independent of real-gas effects. Based on this information, the present analysis determines analytic solutions for nonequilibrium chemistry along streamlines.

The chemical model is that of Ref. 5, i.e., a single Lighthill dissociating gas.[6] The dissociation-recombination reaction represents correctly the controlling chemical mechanism for high-temperature air at IRBM speeds. At higher speeds, a detailed consideration of coupled chemistry is imperative.[2] However, the methods developed here are easily applicable[7] to the full air chemistry. The present work seeks

understanding of chemical relaxation along streamlines. The two main results are the establishment of a simple freezing criterion and the development of a scaling law for nonequilibrium flows. The scaling law is justified by the fact that three-body recombination is a slow process at high altitudes of flight. Its range of validity is determined on the basis of the analytic solutions.

The report is divided into three sections. The first section describes the similitude relationship for binary scaling. Both blunt and slender bodies are considered as well as unsteady blast waves. The second section contains a study of normal shock structure and shows how the chemical relaxation zone behind a normal shock (chemical shock) constitutes a basic element of nonequilibrium flows. Binary scaling of chemical shocks is discussed in a form directly applicable to blunt-body flows. The third section treats two problems. The first problem concerns the mapping of chemical shocks to streamline distributions in blunt-body flows. The accuracy of this procedure is discussed in detail and the freezing criterion is checked. The second problem is the range of validity of binary scaling.

Applications to inviscid nonequilibrium airflows have been carried out[7] and they demonstrate the wide applicability of the present methods. The approach could also be applied to slender bodies. In addition, the extension to include viscous effects is of considerable interest.

SECTION I

BINARY SCALING

Before determining the range of validity of binary scaling, it is useful to note the parameters which control high-speed flows about blunt or slender bodies when chemical rate processes are considered. For binary scaling, the analysis specifies a similitude for nonequilibrium hypersonic flows.

When three-body recombinations are negligibly small, binary scaling is justified as follows. Consider a cold free-stream of density ρ_∞, velocity U_∞, and chemical composition denoted by (α_∞). Assume that the strong hypersonic shock equilibrates only the non-chemical degrees of freedom. The Rankine-Hugoniot conditions give

$$\alpha_s = \alpha_\infty \,, \quad \frac{p_s}{\rho_\infty U_\infty^2} = \frac{2}{\gamma_s + 1} \sin^2 \Theta_s \,, \quad \frac{i_s}{U_\infty^2} = \left[1 - \left(\frac{\gamma_s - 1}{\gamma_s + 1} \right)^2 \right] \sin^2 \Theta_s$$

$$\frac{\rho_s}{\rho_\infty} = \frac{\gamma_s + 1}{\gamma_s - 1} \,, \quad \frac{q}{U_\infty} = \left[\cos^2 \Theta_s + \left(\frac{\gamma_s - 1}{\gamma_s + 1} \right)^2 \sin^2 \Theta_s \right]^{1/2} \tag{1}$$

where Θ_s is the angle of the shock with the free stream and where

$$\gamma_s = \gamma_s \left(U_\infty \,, \alpha_\infty \,, \Theta_s \right) \tag{2}$$

Equation (2) derives from the general property

$$i = i \left(\alpha, T \right) \tag{3}$$

common to the enthalpies of any mixture of ideal gases in vibrational

equilibrium. The result expressed by Eq. (2) plays a basic role in binary scaling, since it allows the shock conditions to be scaled in terms of free-stream density.

The dimensionless variables defined in Eqs. (1) scale exactly the momentum, continuity and energy equations for inviscid flow as well as the state equation. Retaining only binary reaction rates, the chemical rate equations assume the typical form

$$\frac{D\alpha}{Dt} = \rho \, fcn(\alpha, T)$$

and, to scale these equations, the characteristic length, L , of the flow field must satisfy

$$\rho_\infty L = const \tag{4}$$

Equation (4) states the condition for binary scaling. Since this condition preserves the Reynolds number, the viscous flow equations will also scale provided the viscosity coefficients and the Lewis and Prandtl numbers of the various chemical species depend only on (α) and T .

Consider now the boundary conditions at the body. For inviscid flow, L must represent the body scale and the body shape must be kept fixed. For viscous flow, the same requirements handle the case of an insulated and noncatalytic wall. In other cases, the catalytic efficiencies, temperature, and equilibrium concentrations at the wall must also be preserved. Thus, ρ_∞ must be kept fixed unless the wall is cold, [1]

say $T_w < 2000°K$, which is generally true of most practical applications. Before considering in more detail the scaling parameters for inviscid flows, one should note that the above requirements insure scaling of the viscous shock boundary conditions proposed in Ref. 8 for low Reynolds numbers.

The controlling parameters for inviscid nonequilibrium flows about blunt bodies have been discussed in Ref. 1 using the chemical model of a Lighthill gas.[6] The model introduces three numerical data: a dissociation temperature T_d, a rate constant $\bar{C}$ in $cm^3/gm\ sec$ ($\bar{C}$ replaces $C T_d^{-s}$ in Ref. 5) and a characteristic density ρ_d. For fixed $\bar{C}$, the recombination term is proportional to ρ_d^{-1} and binary scaling corresponds to the formal limit $\rho_d = \infty$. Let $v_d = \left(\frac{\mathcal{R} T_d}{\mathcal{M}}\right)^{1/2}$ be a characteristic velocity[6] based on T_d and the molecular weight of the free stream. The relevant Mach number is

$$M_d = \frac{U_\infty}{v_d} \tag{5}$$

If R_N is the radius of the blunt body, the parameter of binary scaling is found to be

$$\Lambda = \frac{\bar{C} R_N \rho_\infty}{U_\infty} \tag{6}$$

Finally, three-body recombination would introduce the altitude parameter

$$\eta = \frac{\rho_\infty}{\rho_d} \tag{7}$$

Thus, nonequilibrium blunt-body flows obey the general similitude

$$V' = fcn\left(\frac{\vec{x}}{R_N} ; M_d , \Lambda , \eta , \alpha_\infty\right) \tag{8}$$

where V' denotes the dimensionless variables $\frac{p}{\rho_\infty U_\infty^2}$, $\frac{T}{M_d^2 T_d}$, $\frac{i}{U_\infty^2}$, $\frac{\rho}{\rho_\infty}$, $\frac{\vec{q}}{U_\infty}$, and α ; $\vec{x}$ is a coordinate vector. For binary scaling, $\eta = 0$. For frozen flow, one sets $M_d = \Lambda = 0$. For equilibrium flow, the Λ dependence drops out of Eq. (8). In the equilibrium limit, the present result agrees with the remark made in Ref. 9 that free-stream pressure and temperature need not be simulated. Furthermore, the Mach number M_∞ based on the sound speed in the free stream becomes a parameter only if the shock cannot be considered as strong.[2] Equation (8) applies to nonequilibrium airflows when reference conditions have been chosen for T_d, $\bar{C}$ and ρ_d.

In the case of slender bodies without nose bluntness, a thickness parameter must also be considered. If L is the body scale and τ the thickness ratio, M_d is replaced by

$$M_d' = \frac{U_\infty \tau}{\nu_d} \tag{9}$$

while the scaling parameter retains the same form

$$\Lambda = \frac{\bar{C} L \rho_\infty}{U_\infty} \tag{10}$$

Then, M_d' , Λ and η control the leading approximation of slender-body theory for nonequilibrium flows

$$V' = \text{fcn}\left(\frac{x}{L}, \frac{y}{Lb}\,;\, M_d', \Lambda, \eta, \alpha_\infty\right) \tag{11}$$

where V' represents the dimensionless variables $\frac{p}{\rho_\infty U_\infty^2 b^2}$, $\frac{T}{M_d^2 T_d}$, $\frac{i}{U_\infty^2 b^2}$, $\frac{\rho}{\rho_\infty}$, $\frac{\tilde{u}}{U_\infty b^2}$, $\frac{\tilde{v}}{U_\infty b}$ and α . Here, $\tilde{u}$ and $\tilde{v}$ are the streamwise and lateral perturbation velocities; x is measured in the streamwise direction and y normal to x . The flow is two-dimensional or axially symmetric. For a wedge or cone

$$y = b\,x$$

and the scale L loses its significance. Equation (11) becomes

$$V' = \text{fcn}\left(\frac{y}{bx}, \frac{\bar{C}\,x\,\rho_\infty}{U_\infty}\,;\, M_d', \eta, \alpha_\infty\right) \tag{12}$$

Again, η = 0 in Eqs. (11) and (12) corresponds to binary scaling.

As noted above, ν_d and $\bar{C}$ assume definite values for non-equilibrium airflows. Thus, the above requirements for binary scaling of inviscid airflows can be summarized

a) fixed body shape

b) $U_\infty b$ = constant (b = 1 for blunt-bodies)

c) $\frac{L\,\rho_\infty}{U_\infty}$ = constant (L length scale of body)

d) fixed composition of the free-stream

Consider now a blunt body with flat-plate afterbody and assume that the chemical concentrations have been established by freezing in the nose region

$$\alpha_f = fcn\left(\frac{\psi}{\rho_\infty U_\infty R_N^{\nu+1}} \; ; \; M_d \, , \, \Lambda \, , \, \eta \, , \, \alpha_\infty\right) \tag{13}$$

where ψ is the stream function and $\nu = 0$, 1 for plane and axisymmetric flows respectively. Equation (13) describes conditions within the entropy layer; in the remainder of the flow, $\alpha = \alpha_\infty$. Neglecting non-chemical contributions to the gas enthalpy, one finds

$$q \approx U_\infty$$

outside of the entropy layer (small perturbation) and

$$\frac{q}{U_\infty} = \sqrt{1 + \frac{2}{M_d}(\alpha_\infty - \alpha_f)}$$

within the entropy layer. Introducing the entropy frozen at the nose

$$\frac{p}{\rho_\infty U_\infty^2}\left(\frac{\rho_\infty}{\rho}\right)^{\gamma_f} = S_f'\left(\frac{\psi}{\rho_\infty U_\infty R_N^{\nu+1}} \; ; M_d \, , \Lambda \, , \, \eta \, , \alpha_\infty\right) \tag{14}$$

with

$$\gamma_f = \gamma_f\left(\frac{\psi}{\rho_\infty U_\infty R_N^{\nu+1}} \; ; M_d \, , \Lambda \, , \eta \, , \alpha_\infty\right) \tag{15}$$

the energy balance of the flow may be expressed. Combining this condition

with the equation for centrifugal pressure drop in the classical blast-wave approach,[10] it is easy to check the following functional form

$$\frac{p_{\text{afterbody}}}{\rho_\infty U_\infty^2} = \text{fcn}\left[\frac{1}{k}\left(\frac{x}{R_N}\right)^{\gamma+1};\ M_d,\ \Lambda,\ \eta,\ \alpha_\infty\right] \tag{16}$$

where k denotes the nose drag coefficient. Equation (16) generalizes Eq. (30) of Ref. 4 in the case of a flat-plate afterbody, (b = 1). Note the dependence of k on M_d, Λ, η and α_∞ as well as the additional dependence introduced in Eq. (16) by the variation of γ_f. For binary scaling, Eq. (16) reduces to

$$\frac{p_{\text{afterbody}}}{\rho_\infty U_\infty^2} = \text{fcn}\left[\frac{1}{k}\left(\frac{x}{R_N}\right)^{\gamma+1};\ M_d,\ \Lambda,\ \alpha_\infty\right]$$

with $k = k(M_d, \Lambda, \alpha_\infty)$. This result expresses the scaling law for afterbody pressure.

It is also interesting to note the application of binary scaling to unsteady blast waves. A blast wave expanding into an atmosphere of density ρ_∞ and creating nonequilibrium flow without recombination is controlled by three numerical data: $\bar{C}\rho_\infty$, v_d, and E the total energy. In distinction from the case of ideal gas flow,[11] the data define a characteristic length

$$L^* = \left(\frac{E}{\rho_\infty v_d^2}\right)^{1/3}$$

so that the blast-wave equivalent to Λ is given by

$$\Lambda^* = \bar{C}\left(\frac{E\,\rho_\infty^2}{v_d^5}\right)^{1/3}$$

The characteristic time scale is

$$t^* = \left(\frac{E}{\rho_\infty v_d^5}\right)^{1/3}$$

and consequently $\frac{p}{\rho_\infty v_d^2}$, α, $\frac{\rho}{\rho_\infty}$, etc. must be functions of $\frac{R}{L^*}$, $\frac{t}{t^*}$, and Λ^* only. Thus, keeping Λ^* fixed insures similitude of the blast wave solutions. For instance, blast waves in air are scaled by maintaining

$$E\,\rho_\infty^2 = \text{const} \tag{17}$$

when three-body recombinations are negligible. The structure of Taylor's solution[11] with its spectacular density drop behind the shock suggests a wide range of validity for Eq. (17).

SECTION II

NORMAL SHOCKS FOR A LIGHTHILL GAS

This section is concerned with an analysis of the relaxation zone for a normal shock in a Lighthill dissociating gas. One seeks a simplified description of normal shock solutions which will point out their role as basic elements of nonequilibrium flow solutions about blunt bodies. The exact solutions for a normal shock is discussed in Section 2.1, in particular the range of validity of binary scaling. Section 2.2 presents an analytic solution for zero recombination which is valid within the scaling range. In Section 2.3, the analytic solution is extended to account for recombination and a uniformly valid solution is developed for the whole shock relaxation zone. This solution will be applied in Section 3 to blunt-body flows.

2.1 Exact Solutions for Normal Shocks

Freeman's analysis[5] assumes a cold incident stream of density ρ_∞ and hypersonic velocity U_∞. Behind a strong, non-chemical shock, the state of the Lighthill gas is given by

$$\frac{\rho}{\rho_\infty} = 7 \qquad \frac{u}{U_\infty} = \frac{1}{7}$$

$$p = \frac{6}{7}\rho_\infty U_\infty^2 \qquad T = \frac{6}{49}\frac{U_\infty^2}{R_o} \tag{18}$$

with $\alpha = 0$. Through the chemical relaxation zone, pressure, density, velocity and internal enthalpy are related by the classical conservation

equations

$$p + \rho u^2 = R_o \rho T(1+\alpha) + \rho u^2 = \rho_\infty U_\infty^2 , \qquad \rho u = \rho_\infty U_\infty$$

$$i + \frac{1}{2} u^2 = (4+\alpha) R_o T + \alpha R_o T_d + \frac{1}{2} u^2 = \frac{1}{2} U_\infty^2 \tag{19}$$

where T_d is the characteristic temperature of dissociation. If C is the rate coefficient and s the temperature exponent of recombination, the rate equation[5] is

$$u \frac{d\alpha}{dx} = \frac{C p}{R} T_d^{-(s+1)} T'^{(s+1)} (1+\alpha)^{-1} \left\{ (1-\alpha) e^{-\frac{1}{T'}} - \alpha^2 \eta \rho' \right\} \tag{20}$$

where $T' = \frac{T}{T_d}$, $\rho' = \frac{\rho}{\rho_\infty}$ and $\eta = \frac{\rho_\infty}{\rho_d}$. Since ρ_d [6] is of order 100 gm/cc, η ranges from 10^{-5} at sea level to 10^{-9} at 200 kft altitude.

For the present application, a new variable is defined

$$\chi = \frac{C}{R T_d^{s+1}} \int_o^x \frac{p\, dx}{u} \tag{21}$$

where $x = 0$ denotes the boundary of the translational shock, and a formal integration of Eq. (20) yields

$$\chi = \int_o^\alpha \frac{(1+\alpha)(T')^{s+1} d\alpha}{(1-\alpha) e^{-\frac{1}{T'}} - \eta \alpha^2 \rho'} = \int_o^\alpha \frac{d\alpha}{F(\alpha, T', \rho'; \eta)} \tag{22}$$

Since T' and ρ' can be expressed in terms of α by means of Eqs. (19), $F(\alpha, T', \rho', \eta)$ becomes a function of the variable α and of the parameters η and $h_\infty = \frac{U_\infty^2}{2 r_d^2}$. Then, the integration may be performed in Eq. (22) to yield $\alpha(\tau)$ for prescribed choices of the parameters. The results are shown in Fig. 1 for $h_\infty = 1$, $s = 2$ and $\eta = 10^{-5}$, 10^{-6}, 10^{-8} and 10^{-9}. One notes the following general property of shock solutions for fixed enthalpy: the solutions corresponding to $\eta \leq \eta_0$ correlate over a significant range of values of τ, $0 \leq \tau \leq \tau_{rec}(\eta_0; h_\infty)$. The table lists values of τ_{rec}, which insure no more than a 1% difference between $\alpha(\tau_{rec}(\eta_0); \eta_0)$ and $\alpha(\tau_{rec}(\eta_0); 10^{-1}\eta_0)$.

TABLE 1

η_0	10^{-5}	10^{-6}	10^{-8}
τ_{rec}	3	10	100

To understand the correlation, consider the curves labelled R_1 in Fig. 1 which show the ratio of recombination rate to dissociation rate for the various shock solutions.

$$R_1(\tau; \eta, h_\infty) = \frac{\alpha^2}{1-\alpha}\, \eta \rho' e^{\frac{1}{T'}}$$

Over the range $0 \leq \tau \leq \tau_{rec}(\eta_0)$, R_1 is smaller than 0.3. In fact, the rise of R_1 to 0.3 is achieved very suddenly[1] as evidenced

by the R_1 - curves.[4] Hence, when $0 \leq \chi \leq \chi_{rec}$, chemical recombination cannot affect the concentration field. The altitude dependence introduced by η drops out of the problem and the shock solutions may be scaled for free-stream density. Then, α is only a function of χ and h_∞.

2.2 Analytic Solution for Zero Recombination

The use of the variable χ allows a direct application of the shock solution to other flow problems. Consider first the range $0 \leq \chi \leq \chi_{rec}$. Through the shock relaxation zone, the internal enthalpy remains nearly constant because $\left(\frac{u}{U_\infty}\right)^2$ is small compared to one and Eq. (22) can be approximated by

$$\chi = \int_0^\alpha \frac{1+\alpha}{1-\alpha} (T')^{s+1} e^{\frac{1}{T'}} d\alpha \approx \int_0^\alpha \frac{1+\alpha}{1-\alpha} \left(\frac{h_\infty - \alpha}{4+\alpha}\right)^{s+1} \exp\left(\frac{4+\alpha}{h_\infty - \alpha}\right) d\alpha \qquad (23)$$

Equation (23) provides a formal solution of the rate equation for zero recombination and a fixed enthalpy. Several important flows satisfy this last requirement. For instance, Newtonian theory for blunt-body flows predicts constant enthalpy along streamlines. More generally, in the subsonic region of a blunt-body flow, the enthalpy is nearly uniform because of low fluid velocities. Another example is that of inviscid wedge flows for which the pressure variations are negligible. In such cases, the required interpretation of χ is

$$\tau \Longrightarrow \frac{C}{RT_d^{s+1}} \int_0^{\sigma} \left(\frac{p\,d\sigma}{q}\right)_{\substack{\text{along a}\\ \text{streamline}}} \tag{24}$$

where σ denotes the arc length along a streamline, measured from the shock and q is the flow velocity. An a priori knowledge of the function τ can be obtained from Newtonian theory as discussed in Section 2.1.

The function

$$I(\alpha;h) = \int_0^{\infty} \frac{1+\alpha}{1-\alpha} \left(\frac{h-\alpha}{4+\alpha}\right)^{s+1} \exp\left(\frac{4+\alpha}{h-\alpha}\right) d\alpha \tag{25}$$

plays an important role in the theory of nonequilibrium flows. It is plotted in Fig. 2 for $0.2 \leq h \leq 1$ and $s = 2$, a choice suggested by the experimental results of Ref. 12 for oxygen dissociation. The dashed lines of Fig. 2 will be discussed later. As α tends to h, $I(\alpha;h)$ becomes infinite. The asymptotic behavior is found by integrating by parts the rapidly varying exponential term,

$$I(\alpha;h) \sim \left(\frac{1+\alpha}{1-\alpha}\right) \frac{(h-\alpha)^{s+3}}{(4+h)(4+\alpha)^{s+1}} \exp\left(\frac{4+\alpha}{h-\alpha}\right)\left\{1 + O(h-\alpha)^2\right\} \tag{26}$$

Along the steep parts of the I curves, a large increase of τ has little effect on α, a circumstance which suggests chemical freezing (cf. Section 2.3). By comparing Figs. 1 and 2, one finds that the

"dissociation" solution

$$\chi = I(\alpha ; h) \tag{27}$$

agrees very well with the shock solutions for $0 \leq \chi \leq \chi_{rec}$ For a very high enthalpy, $h_\infty = 3$, which is not shown in Fig. 2, the agreement is complete including the final equilibrium value $\alpha_e \approx 1$. Indeed the dissociation rate vanishes for $\alpha = 1$ so that, when $\alpha_e \approx 1$, the neglect of recombination will provide a uniformly valid solution for all χ Then, dissociation scaling applies[5] in the whole shock. Figure 3 presents the function $I(\alpha ; h)$ for $s = 0$. These curves will be used in the comparison with airflows discussed in Section 3.6.

2.3 Analytic Solution Including Recombination

When $\alpha_e < 1$, a sizeable χ - range of the shock transition cannot be scaled and the problem is to render Eq. (27) uniformly valid. To achieve this, one notes that R_1 is a very sensitive function of α [5] When the enthalpy remains constant, the condition $R_1 = 1$ determines the infinite-rate equilibrium solution corresponding to the given pressure field, say $\alpha_{e,\infty}$. As shown in Fig. 1, R_1 is generally very small and rises to one in a small neighborhood of $\alpha_{e,\infty}$. For $\alpha - \alpha_{e,\infty} \ll 1$, the function F of Eq. (22) can be approximated by

$$F \sim \left(\frac{4+\alpha_{e,\infty}}{h-\alpha_{e,\infty}}\right)^{s+1} \frac{1-\alpha_{e,\infty}}{1+\alpha_{e,\infty}} \left\{ \exp\left(-\frac{4+\alpha}{h-\alpha}\right) - \exp\left(-\frac{4+\alpha_{e,\infty}}{h-\alpha_{e,\infty}}\right) \right\}$$

where only the variation of the exponential term is preserved. Using

$\gamma = \frac{1}{T'}$ as a variable, one obtains the asymptotic behavior for large γ

$$\tau \sim A \int^{\gamma} \frac{d\gamma}{e^{-\gamma} - e^{-\gamma_\infty}}, \quad A = \frac{1+\alpha_{e,\infty}}{1-\alpha_{e,\infty}} \frac{(h-\alpha_{e,\infty})^{s+3}}{(4+h)(4+\alpha_{e,\infty})^{s+1}} \tag{28}$$

Hence

$$\tau \sim -A e^{\gamma_\infty} \log\left(1 - e^{\gamma-\gamma_\infty}\right) \approx -I(\alpha_{e,\infty}; h) \log\left[1 - \exp\left(\frac{1}{T'} - \frac{1}{T'_\infty}\right)\right]$$

since $I(\alpha_{e,\infty}; h)$ is generally so large that Eq. (26) may be applied. Now $\exp\left(\frac{1}{T'} - \frac{1}{T'_\infty}\right)$ is equal to the ratio of recombination rate to dissociation rate when T' is close to $T'_{e,\infty}$, i.e., when R_1 is of order one, and the function may be approximated by

$$\frac{1-\alpha}{1+\alpha} (T')^{s+1} e^{-\frac{1}{T'}} \exp\left[-\frac{\tau}{I(\alpha_{e,\infty}; h)}\right]$$

with good accuracy for both small and large τ. Finally, the differential form of Eq. (22) becomes

$$dI(\alpha; h) = \exp\left[-\frac{\tau}{I(\alpha_{e,\infty}; h)}\right] d\tau$$

or

$$I(\alpha; h) = I(\alpha_{e,\infty}; h) \left[1 - \exp -\left(\frac{\tau}{I(\alpha_{e,\infty}; h)}\right)\right] \tag{29}$$

Equation (29) has been derived under the tacit assumption of constant $\alpha_{e,\infty}$, i.e., of constant pressure. When the pressure varies, one finds that $I(\alpha_{e,\infty}; h)$ is a slowly varying function of the physical coordinates, say σ, as compared with $\tau(\sigma)$. Hence, $\frac{dI[\alpha_{e,\infty}(\sigma); h]}{d\tau(\sigma)}$

is small and the above result is still valid so that Eq. (29) may be applied for a variable equilibrium concentration, $\alpha_{e,\infty}(\sigma)$. This result recovers the correct equilibrium limit for $\chi \gg 1$ and the correct behavior for small χ (dissociation solution). It compares accurately with exact shock solutions for all values of χ and for $\eta \leq 10^{-6}$.

Equation (29) provides a convenient tool for the study of nonequilibrium flows when the assumption of constant enthalpy is correct. The formal analogy with linearized solutions of chemical relaxation is particularly satisfying.

SECTION III

APPLICATION TO BLUNT-BODY FLOWS

The normal shock solutions are now adapted to describe nonequilibrium flow about blunt bodies. The adaptation is based on the Newtonian Theory for pressure and velocity distributions which is reviewed in Section 3.1. The limiting case of equilibrium flows is considered in Section 3.2 and the limit of small recombination is analyzed in Section 3.3. Next, a more detailed study of the rate process is developed. It reveals the existence of a nonequilibrium sublayer near the shock (Section 3.4) followed by a region of small α variations (Section 3.5). Finally, Section 3.6 applies the results to determine the range of validity of binary scaling.

3.1 Newtonian Theory

The analytic approach is now applied to nonequilibrium flow of an ideal dissociating gas around a blunt body. An a priori knowledge of the "transit time" $\chi \sim \int_0^\sigma \frac{\rho d\sigma}{g}$ and of the infinite rate equilibrium solution is required. Newtonian flow theory[5, 13] provides the basic data. If $1/\epsilon$ is the (large) compression ratio across a hypersonic shock, the following classical results are subject to errors of nominal order ϵ : velocity and enthalpy remain constant along a streamline and the pressure field is given in terms of shock shape (or body shape in this approximation).

Furthermore, the streamlines remain close to the shock (thin shock layer). These results apply for both ideal and nonequilibrium gas flows.

In the subsonic region behind the bow shock, the error in velocity becomes of order $\sqrt{\epsilon}$. It may be corrected in the manner of Freeman.[13] However, α is then close to stagnation equilibrium since the flow is assumed to be inviscid and an accurate determination of η is not critical. In the supersonic region, the Newtonian pressure generally vanishes along a singular line (starting at 60° on a spherical body). To remove this singularity is difficult[14] and one may prefer to interpret it as a symptom of shock-layer detachment.[6] For the present purpose, one takes $p \approx 0$ beyond the zero pressure line so that η has a finite maximum for all but the body streamline. At the stagnation point, η becomes infinite.

The Newtonian approximation of constant enthalpy along a streamline is inaccurate for the computation of certain real gas effects. Indeed, the exponential term, $e^{-\frac{1}{T'}}$, which appears in the rate equation and in the equilibrium constant is quite sensitive to enthalpy for a given concentration. The error in the argument is of order $\epsilon/T' \approx 0(1)$, as $T' < 0.2$ in most applications. Fortunately, the enthalpy drop along a streamline can be determined in terms of the zero-order Newtonian solution for pressure. The associated velocity rise affects only the transit time η on which α depends rather weakly. Thus, including the enthalpy drop, the expected accuracy of the concentration field is of order ϵ

The example chosen is that of a spherical shock cap of radius R_s for which Freeman's [13] solution is available

$$p' = \frac{p}{\rho_\infty U_\infty^2} = \frac{\sin 3\vartheta + \sin^3 \xi}{3 \sin \vartheta} , \qquad q' = \frac{q}{U_\infty} = \sin \xi$$

$$\tau = \frac{C T_d^{-(s+1)}}{R} \int_0^\sigma \frac{p \, d\sigma}{q} = \tag{30}$$

$$\frac{\bar{\Lambda}}{3 \sin \xi} \left\{ \vartheta - \xi + \sin 2\vartheta - \sin 2\xi + \sin^3 \xi \log \frac{\operatorname{tg} \frac{1}{2}\vartheta}{\operatorname{tg} \frac{1}{2}\xi} \right\}$$

The basic nonequilibrium parameter of the present analysis is

$$\bar{\Lambda} = \frac{C R_s \rho_\infty T_d^{-(s+1)} U_\infty}{R_o} \tag{31}$$

It is simply related to Freeman's parameter Λ . The angle ξ locates the point at which a streamline crosses the shock and ϑ is the running angle coordinate. Both angles are measured from the axis (see Fig. 4). The stagnation streamline is obtained when ϑ and ξ both tend to zero for a given limit of $\frac{\vartheta}{\xi}$. Ideal flow of the Lighthill gas corresponds to $\bar{\Lambda} \rightarrow 0$, whereas equilibrium flow obtains for large values of $\bar{\Lambda}$. In the absence of dissociation in the free stream, two other parameters control the blunt-body nonequilibrium flow: the enthalpy ratio $h_\infty = \frac{1}{2} M_d^2$ and the density ratio $\eta = \frac{\rho_\infty}{\rho_d}$. The purpose of the subsequent analysis is to classify flow regimes according to the values of $\bar{\Lambda}$ and η for $h_\infty = 1$ (5.5 Km/sec in O_2).

3.2 Equilibrium Flows

For equilibrium flows, the recombination rate plays a dominant role and binary scaling cannot apply. Then, the body size no longer controls the concentration field and the problem is to ascertain the altitude dependence of equilibrium concentrations.

The analysis uses an approximate solution which demonstrates the following striking features also noted in equilibrium airflows

(1) at fixed enthalpy, the concentrations[15] depend very weakly on density.

(2) at fixed entropy,[16] the pressure dependence is weak.

Consider now a Lighthill gas. Let (T_1' , α , h_1 , p_1) and (T_2' , α_2 , h_2 , p_2) be two solutions of the equilibrium equations

$$\frac{\alpha^2}{1-\alpha^2} = \frac{p_d}{p}\, T' \exp\left(-\frac{1}{T'}\right), \qquad h = (4+\alpha)T' + \alpha \tag{32}$$

$$dh = \nu\, T'(1+\alpha)\, d(\log p)$$

with $\nu = 0$ for case 1 and $\nu = 1$ for case 2. Expecting small differences between (α_1 , α_2) and (T_1' , T_2') respectively, one assumes

$$\alpha_2 = \alpha_1 \left[1 + a \log \frac{p_2}{p_1}\right] , \quad T_2' = T_1' \left[1 + b \log \frac{p_2}{p_1}\right] \tag{33}$$

with a , $b \ll 1$. Then

$$h_2 = h_1 + \nu T_1'(1+\alpha_1)\log\frac{p_2}{p_1} + O(aT_1', bT_1')\nu\log^2\frac{p_2}{p_1}$$

and by substitution into Eqs. (32)

$$a = \frac{\nu T_1'(1+\alpha_1)(1+T_1') - (4+\alpha_1)T_1'^2}{\alpha_1 + 2\alpha_1 T_1' + \left(\alpha_1 + 2\frac{4+\alpha_1}{1-\alpha_1^2}\right)T_1'^2}$$

$$b = \frac{T_1'}{1+T_1'} + \frac{2aT_1'}{(1-\alpha_1^2)(1+T_1')} \qquad (34)$$

For equilibrium flows and moderate enthalpies, $h \leq 1$, T_1' is smaller than 0.1 and one may expand in powers of T_1'. The present solution is subject to an error of order $T_1'^2$ or $T_1'^3$ for a if $\nu = 0$; a and b are at most of order T_1' so that the weak logarithmic dependence on pressure is further reduced by small coefficients. At fixed enthalpy, a is of order $T_1'^2$ and the pressure dependence becomes even weaker (case 1). If the flow is isentropic, α is controlled by enthalpy changes whereas T' is quite insensitive. Hence, a shock-layer solution for equilibrium concentration must account for the enthalpy drop.

It is interesting to note that, by combining Eqs. (33) with the state equation, one recovers the concept of adiabatic exponent[17] for equilibrium flow

$$\frac{p_2}{p_1} \approx \left(\frac{\rho_2}{\rho_1}\right)^{\gamma'}, \qquad \gamma' = \left(1 - \frac{\alpha_1 a}{1+\alpha_1} - b\right)^{-1} \qquad (35)$$

If the flow is isentropic, the ideal gas limit, $\gamma' = 4/3$, is recovered as α_1, $T_1' \longrightarrow 0$ whereas $\gamma' = 5/3$ for $\alpha_1 = 1$ and any T_1' Equations (34) are accurate over a pressure drop by a factor of the order 10. They may be applied along streamlines with given equilibrium shock conditions (α_1, T_1', h_1, ρ_1).

3.3 Newtonian Solution for Small Recombination

At high altitudes of flight, the density ratio η which controls chemical recombination is very small and one expects recombination to have a negligible effect on the concentration field except in the close neighborhood of the stagnation point where equilibrium must obtain in inviscid flow. Then, η is no longer a parameter of the problem and, if $\bar{\Lambda}$, h_∞, and the shock shape (or body shape) are kept fixed, the nonequilibrium solutions will scale[1] for body size and free stream density. For airflows with a fixed chemical model, the scaling requirements are that $\rho_\infty R_s$, U_∞ and the shock shape (or body shape) remain fixed. Successful correlations of blunt-body airflows[1, 2] have been demonstrated. For a Lighthill dissociating gas, keeping $\bar{\Lambda}$ and h_∞ fixed also transforms from one Lighthill gas to another.

As noted in Section 2.2, a simple solution is readily obtained for zero recombination under the Newtonian assumptions. It is given by

$$I(\alpha; h) = \bar{\Lambda} \int_0^{\sigma'} \frac{p' d\sigma'}{g'} \tag{36}$$

where σ' is the dimensionless arc length measured along a streamline starting at the shock. For the spherical shock of Section 3.1, one finds

$$h = h_\infty \cos^2\xi\,, \qquad I(\alpha, h_\infty \cos^2\xi) = \bar{\Lambda}\,\zeta(\vartheta, \xi)$$

$$\zeta(\vartheta,\xi) = \frac{\vartheta - \xi + \sin 2\vartheta - \sin 2\xi + \sin^3\xi \log\left(\operatorname{tg}\tfrac{1}{2}\vartheta / \operatorname{tg}\tfrac{1}{2}\xi\right)}{3\sin\xi} \tag{37}$$

Equations (37) determine the concentration field for a prescribed choice of h_∞ and Λ (see Fig. 2 for $I(\alpha, h)$). Figure 5 gives a plot of the coordinate $\zeta(\vartheta, \xi)$ for a typical streamline corresponding to $\xi = 0.5$; the curve stops at shock-layer detachment ($\sin 3\vartheta_{max} = -\sin^3\xi$) where ζ attains its maximum value $\zeta_{max}(\xi)$. One notes the rapid rise of ζ to its maximum value. This result suggests that the unrealistic behavior of the Newtonian solution near shock-layer detachment will not compromise the solution for nonequilibrium concentration field.

The function $\zeta_{max}(\xi)$ is plotted as the full curve of Fig. 6. At the body, ζ_{max} is infinite. Close to the body, $\vartheta_{max} \approx \frac{\pi}{3}$ and one may use the approximation

$$\zeta_{max} \approx \frac{\vartheta_{max} + \sin 2\vartheta_{max}}{3\xi} - 1 \approx \frac{0.64}{\xi} - 1 \tag{38}$$

For $\xi > 10°$, ζ_{max} is of order one. It becomes very small near $\xi = \frac{\pi}{2}$ to provide a practical cutoff of dissociation when the shock is no longer strong. On each streamline, the maximum value of α is given by

$$I(\alpha_{max}, h_\infty \cos^2\xi) = \bar{\Lambda}\,\zeta_{max}(\xi) \tag{39}$$

Figure 7 shows the profiles of $\alpha_{max}(\xi)$ for $h_\infty = 1$ and $\bar{\Lambda} = 10$, 10^2, 10^3, and 10^4. These results define the final levels established by dissociation freezing in expansion around the blunt body. They apply when chemical recombination is very small, i.e., at high altitudes of flight. For a fixed enthalpy (fixed ξ) the concentration depends weakly on the rate parameter $\bar{\Lambda}$, an order of magnitude increase of $\bar{\Lambda}$ corresponding only to a 10% rise in α_{max}. This feature has been previously noted in numerical solutions for nozzle flows[18] where freezing occurs in a flow initially in chemical equilibrium. The dashed curves in Figs. 6 and 7 will be discussed later.

Since recombination has been neglected, α_{max} tends to $h_\infty = 1$ as $\xi \longrightarrow 0$, rather than to the stagnation equilibrium level. For higher values of h_∞, say $h_\infty \approx 3$, the dissociation solution of Eq. (37) still gives $\alpha_{max}(0) = 1$, since $I(\alpha, h_\infty)$ first becomes infinite at $\alpha = 1$ (see Section 2.2) rather than at $\alpha = h_\infty$. The result $\alpha_{max}(0) = 1$ is, in fact, correct because stagnation equilibrium corresponds to full dissociation for such high enthalpies. Then, recombination can be neglected even at the stagnation point.[1] Under such extreme conditions, however, the physical significance of the Lighthill gas model is open to doubt.

At lower enthalpies, chemical recombination must be included near the stagnation point even when η is very small. To account for it, one may apply a normal shock solution as explained in Section 2.2.

For the present case $h_\infty = 1$, the shock solutions plotted in Fig. 1 are appropriate since the method is justified only for streamline enthalpies close to h_∞. Figure 8 shows the concentration profiles obtained for $\eta = 10^{-8}$ (about 150 kft altitude) and $\bar{\Lambda} = 10,\ 10^2$. Using the notation of Section 2.2, one finds

$$\tau_{rec}\,(\eta = 10^{-8}\,,\ h_\infty = 1) \approx 100$$

The criterion is then

$$\zeta_{rec} \approx \frac{100}{\bar{\Lambda}}$$

and, for streamlines such that $\zeta_{max} < \zeta_{rec}$, recombination can be neglected. Thus, for $\bar{\Lambda}$ in the range 10^3, 10^4, one would predict that recombination would affect the whole flow field, whereas, for $\bar{\Lambda}$ in the range 10, 10^2, the effect is concentrated in a small region near the body. Note that $\alpha_{max}\,(0)$ remains constant along the body which requires immediate freezing after the stagnation point. The work of Ref. 19 verifies this assumption.

The above solution is subject to two main sources of errors. The solution without recombination does not allow for enthalpy drop along a streamline while the adaptation of the normal shock solution in addition neglects the decrease of recombination rate with streamline pressure. The first error over-estimates dissociation rates whereas the second one exaggerates recombination rates. It is interesting to study the interplay of these two causes of error and to obtain solutions when recombination is important over the whole flow field. This purpose requires a closer study of the freezing process.

3.4 Nonequilibrium Sublayer with Recombination

The process of chemical relaxation along a blunt-body streamline occurs in two distinct stages. The first stage develops within a non-equilibrium sublayer close to the shock for which pressure and enthalpy remain essentially fixed at shock conditions. This sublayer is analyzed below. The second stage occurs during the flow expansion around the blunt body; it corresponds to small α - variations and may be described by the exact solution of Section 3.5.

Consider Fig. 9 which is based on the dissociation solution of Section 3.3. Two typical α - profiles are shown along streamlines which have the same enthalpy. Curve a is obtained for a low value of $\bar{\Lambda}$; α rises slowly to its final value. In case b , one observes a sharp rise behind the shock followed by a slow final increase. Case b is of main interest as it corresponds to much higher final concentrations. The solution then displays the typical behavior of chemical freezing which is intuitively assigned to the point where

$$\frac{d\alpha}{d\zeta}(\alpha, \bar{\Lambda}, h) = \bar{\Lambda} T'^{-(s+1)} \frac{1-\alpha}{1+\alpha} e^{-\frac{1}{T'}} = 1 \tag{40}$$

Let α_o , T_o' and ζ_o be the coordinates of this point; α_o and T_o' depend only on $\bar{\Lambda}$ and h and the definition is independent of the type of solution considered. In a general case where recombination may be effective, the conditions (T_o' , α_o) still represent a "turning point" for the dissociation rate. Indeed, the controlling factor is $\bar{\Lambda} \exp\left(-\frac{1}{T'}\right)$,

which may be approximated as $\exp\left(\frac{T'-T_0'}{T_0'^2}\right)$; T_0' is small compared to one so that the dissociation rate is finite only in a small range near T_0'. This rate is large if $T'-T_0' \gg T_0'^2$ (sharp rise near the shock) and small when $T_0'-T' \gg T_0'^2$ (slow final rise). Thus, dissociation freezing will occur only for T' close to T_0'.

The functions $\alpha_0(\bar{\Lambda}, h)$ and $T_0'(\bar{\Lambda}, h)$ are plotted in Figs. 10 and 11 for the present choice $s = 2$ of the temperature exponent of the recombination rate. The dashed curve of Fig. 11 defines the values of $\bar{\Lambda} = \bar{\Lambda}_1(h)$ such that $T_0' = T_s'$ for ideal gas conditions, i.e. $T_0' = \frac{h}{4}$. Case b) of Fig. 9 corresponds to points above the dashed curve of Fig. 11. To discuss possible freezing, one must evaluate the recombination rate $r_R(\zeta_0)$. When the rate equation is expressed in terms of the variable ζ, $r_R(\zeta)$ is given by $\frac{\alpha^2}{1+\alpha}\eta\rho' T'^{-(s+1)}$ and if $p(\zeta_0) \approx p_s = 4R_0\rho_\infty T_d h$ by the strong shock conditions, one finds

$$r_R(\zeta_0) = 4\eta h \frac{\alpha_0^2}{1-\alpha_0^2} T_0' e^{\frac{1}{T_0'}} = 4\eta h \bar{\Lambda}\left[\frac{\alpha_0}{(1+\alpha_0)T_0'}\right]^2 \qquad (41)$$

The function $10^{-s}\frac{r_R(\zeta_0)}{\eta}(\bar{\Lambda}, h)$ is plotted in Fig. 12 which serves to define the values of $\bar{\Lambda} = \bar{\Lambda}_2(h, \eta)$ for which T_0' is equal to equilibrium shock temperature (i.e. $r_R(\zeta_0) = 1$). These values are listed in the following table:

TABLE 2

h	1	0.8	0.6	0.4
$\bar{\Lambda}_2(h, 10^{-6})$	150	250	500	1800
$\bar{\Lambda}_2(h, 10^{-7})$	950	1500	3000	10^4

For a chosen altitude (η fixed), the range of primary interest for nonequilibrium flow along a streamline is $\bar{\Lambda}_1 \leq \bar{\Lambda} \leq \bar{\Lambda}_2$ If $\bar{\Lambda} < \bar{\Lambda}_1$, case a of Fig. 9 obtains and the gas may be considered as nearly ideal. If $\bar{\Lambda} \geq \bar{\Lambda}_2$, the flow is in chemical equilibrium. Figure 12 also reveals a marked decrease of $\kappa_R(\zeta_0)$ for fixed $\bar{\Lambda}$ and decreasing h . Hence, the method of Section 3.3 which predicts the range of influence of recombination on the basis of the stagnation shock solution may be conservative.

One should now ascertain the sublayer character of the region under consideration. Its existence has been tacitly assumed since enthalpy and pressure have been kept fixed at shock conditions. To estimate ζ_0 for small recombination, a steepest descent evaluation of $I(\alpha, h)$ may be used

$$\zeta_0 = \frac{1}{\bar{\Lambda}} I(\alpha_0, h) = \frac{1}{\bar{\Lambda}} \int_{T_0'}^{h/4} \frac{h+4}{(1+T')^2} \frac{1+h-3T'}{1-h+5T'} T'^3 e^{\frac{1}{T'}} dT'$$

$$\approx \frac{4+h}{(1+T_0')^2} \int_{T_0}^{h/4} \exp \frac{T_0'-T'}{(T_0')^2} dT' \leq \frac{(4+h)T_0'^2}{(1+T_0')^2} \qquad (42)$$

This value is generally small since T_0' is small and $(4 + h)\, T_0'$ is at most of order one. In the sublayer, recombination may be important for large values of $\bar{\Lambda}$ and a more precise evaluation of ζ_0 makes use of the appropriate normal shock solution. The results listed in the following table are obtained by combining Figs. 1 and 10 for the representative case $\eta = 10^{-8}$, $h = 1$.

TABLE 3

$\bar{\Lambda}$	10	10^2	10^3	3×10^3
ζ_o	0.13	0.07	0.05	0.03

As $\bar{\Lambda}$ increases, ζ_o decreases and the concentration rise behind the shock becomes sharper. Since $\frac{d\zeta}{d\sigma'} \geq O(1)$, σ_o' is even smaller. In the supersonic region, σ_o' is measured in a direction parallel to the shock (Newtonian streamlines) along which fluid properties vary slowly in the sense of the shock-layer approximation. In the subsonic region, pressure and enthalpy vary slowly in all directions. Hence, the sublayer assumptions are justified and, if the flow reaches equilibrium in the sublayer, the equilibrium level must be that prevailing at the shock. Thus, Eq. (29) is accurate within the sublayer.

3.5 Exponential Approximation

Consider now the chemical process beyond the turning point, i.e., in the range $T' < T_o'$ for any given streamline. Two possibilities may occur

1. Freezing before reaching equilibrium
2. Equilibrium flow

Case 1 is described in Section 3.3 with the assumption of constant enthalpy. Comparing Figs. 7 and 10 shows that the final frozen level is always close to α_o. The inclusion of enthalpy drop and recombination enhance this result. For case 2, the study of Section 3.3 shows small perturbations from shock equilibrium conditions which must be close to (α_o, T_o') if equilibrium is to be attained.

The analysis assumes small perturbations from (α_o , T_o') together with the exponential approximation introduced in Section 3.4. The basic equations become

$$\frac{\partial \alpha}{\partial \zeta} = \exp \frac{T' - T_o'}{T_o'^2} - \beta_o \frac{p}{p_o}$$

$$h = (4 + \alpha_o) T' + \alpha \tag{43}$$

$$\frac{\partial h}{\partial \zeta} = T_o' (1 + \alpha_o) \frac{\partial \log p}{\partial \zeta}$$

where $\beta_o = \kappa_R(\zeta_o)$ is the recombination rate at the turning point (see Fig. 12). Combining the second and third Eqs. (43), one finds

$$h = h_o + T_o'(1 + \alpha_o) \log \frac{p}{p_o} = (4 + \alpha_o) T' + \alpha \tag{44}$$

and, substituting for T' in the first equation, one obtains an equation for α

$$\frac{\partial \alpha}{\partial \zeta} = \left(\frac{p}{p_o}\right)^{\mu_o} \exp \frac{\alpha_o - \alpha}{(4 + \alpha_o) T_o'^2} - \beta_o \left(\frac{p}{p_o}\right) \tag{45}$$

with

$$\mu_o = \frac{1 + \alpha_o}{(4 + \alpha_o) T_o'} \tag{46}$$

Equation (45) suggests the use of small perturbation variables

$$\bar{\alpha} = \frac{\alpha - \alpha_o}{(4 + \alpha_o) T_o'^2} \quad , \quad \bar{\zeta} = \frac{\zeta - \zeta_o}{(4 + \alpha_o) T_o'^2} \quad , \quad (4 + \alpha_o) T_o'^2 \ll 1 \tag{47}$$

giving

$$\frac{\partial \bar{\alpha}}{\partial \bar{\zeta}} = \left(\frac{p}{p_0}\right)^{\mu_0} \exp(-\bar{\alpha}) - \beta_0 \frac{p}{p_0} \tag{48}$$

The boundary condition insures matching of the present solution with the sublayer distribution

$$\bar{\zeta} = 0 \quad : \quad \bar{\alpha} = 0 \tag{49}$$

In Eq. (48), $\frac{p}{p_0}$ is a known function of ζ through Eqs. (30) and (37).

Equation (48) has an explicit solution

$$\bar{\alpha} = \log\left[1 + \lambda_0 \int_{\zeta_0}^{\zeta} \left(\frac{p}{p_0}\right)^{\mu_0} \exp\left(\delta_0 \int_{\zeta_0}^{\zeta} \frac{p}{p_0}\, d\zeta\right) d\zeta\right] - \delta_0 \int_{\zeta_0}^{\zeta} \frac{p}{p_0}\, d\zeta \tag{50}$$

where, for convenience, the following parameters have been introduced

$$\lambda_0 = \frac{1}{(4+\alpha_0)\,T_0'^2} \gg 1 \quad , \quad \delta_0 = \frac{\beta_0}{(4+\alpha_0)\,T_0'^2} \tag{51}$$

Since ζ_0 is small compared to $\zeta_{max}(\xi)$, the solution may be applied in a more convenient form

$$\bar{\alpha} = \log\left[1 + \lambda_0 \int_{0}^{\zeta} \left(\frac{p}{p_0}\right)^{\mu_0} \exp\left(\delta_0 \int_{0}^{\zeta} \frac{p}{p_0}\, d\zeta\right) d\zeta\right] - \delta_0 \int_{0}^{\zeta} \frac{p}{p_0}\, d\zeta \tag{52}$$

the turning point being approximated by $\zeta = 0$.

Equation (52) reveals a number of interesting features of non-equilibrium flows. The infinite rate equilibrium limit is obtained from Eq. (48) by solving

$$\exp(-\bar{\alpha}) = \beta_0 \left(\frac{p}{p_0}\right)^{1-\mu_0} = \left(\frac{p}{p_0}\right)^{1-\mu_0} \tag{53}$$

since $\beta_0 = 1$ for infinite rate equilibrium. Hence

$$\alpha_{e,\infty} = \alpha_1 + \left[(1+\alpha_1)T_1' - (4+\alpha_1)T_1'^2\right] \log \frac{p}{p_1} \tag{54}$$

where (α_1 , T_1') describe equilibrium at the shock. The coefficient of $\log \frac{p}{p_1}$ in Eq. (54) compares well with the more exact Eq. (35) of Section 3.2. This result could be expected since Eq. (54) derives from Eq. (35) by neglect of $O(T_1'^2) \ll 1$. When β_0 is different from one, Eq. (53) defines the local equilibrium which is very close to infinite rate equilibrium whenever β_0 is of order one. The infinite rate equilibrium is also recovered from Eq. (52) by letting δ_0 tend to infinity for $\beta_0 = \frac{\delta_0}{\lambda_0} = 1$.

The other limiting case is that of the dissociation solution, $\beta_0 = 0$, obtained in the spirit of Section 3.3. One finds

$$\alpha(\zeta_{max}; \beta = 0) = \alpha_0 + (4+\alpha_0)T_0'^2 \log\left[1 + \lambda_0 \int_0^{\zeta_{max}} \left(\frac{p}{p_0}\right)^{\mu_0} d\zeta\right] \tag{55}$$

The pressure dependence accounts for the enthalpy drop along streamlines which was previously neglected. To test the exponential approximation,

one may compare the final frozen levels obtained by setting $\mu_o = 0$, $\zeta = \zeta_{max}(\xi)$ to those obtained in Fig. 7 for $\bar{\Lambda} = 10, 10^2, 10^3, 10^4$. The comparison is shown as the dashed curves of Fig. 7. It is satisfactory except in the neighborhood of the body where the dissociation solution of Section 3.3 must also fail. When using Eq. (55), one takes $\alpha = 0$ for streamlines where $T_o' > T_s' = \frac{1}{4} h_o$ (case *a* of Fig. 9). Figure 6 shows this to be correct.

3.6 Range of Validity of Binary Scaling

The above comparisons give confidence in Eq. (52) which describes accurately both dissociation freezing and equilibrium flow. Equation (52) is now applied to discuss the transition. The range of validity of binary scaling is found by comparing nonequilibrium flows for the same body shape, the same flight speed ($h_\infty = 1$), the same value of $\bar{\Lambda}$ and for increasing values of η. For a fixed streamline, the recombination rate at the turning point, $r_R(\zeta_o ; \eta)$, increases with η. If $r_R(\zeta_o ; \eta) < 0.3$, three-body recombination does not affect the nonequilibrium sublayer (cf. Section 2.2) and there exists a possibility of scaling the whole concentration field with the exception of a small region near the stagnation point. If $r_R(\zeta_o ; \eta) \geq 0.3$ the sublayer approaches chemical equilibrium. However, α_o does not depend on η and changes of α beyond the turning point are expected to be small (cf. Section 3.5). Hence, for $\zeta \gg \zeta_o(\xi ; \bar{\Lambda}, \eta)$, $\alpha(\zeta ; \xi, \bar{\Lambda}, \eta)$ should have only a weak dependence on η for fixed $\bar{\Lambda}$, and ξ. Here, one considers the scaling

range

$$r_R(\zeta_o ; \eta) < 0.3$$

It is then required to check the solution of Section 3.3 which was transcribed from a normal shock.

Equation (52) may be evaluated numerically for a given pressure distribution and for a prescribed shock shape. The use of a Newtonian solution for $\frac{p}{p_o}(\zeta)$ is not essential as long as the pressure field remains unaffected by the chemical processes. As checked in Ref. 7, this prediction of Newtonian theory appears to have a wide range of validity. Most of the subsequent analysis assumes a linear pressure variation

$$\frac{p}{p_o} = 1 - \bar{A}\,\zeta\,, \qquad \bar{A} = \frac{3\sin^2\xi}{\cos^3\xi} \tag{56}$$

with the pressure gradient defined at the shock by the Newtonian solution. The assumption is particularly justified for evaluating the log term in Eq. (45). A numerical study shows that $\mu_o(\bar{\Lambda} ; h_o)$ is practically a function of $\bar{\Lambda}$ only and takes on high values (cf. Table 4).

TABLE 4

$\bar{\Lambda}$	10	10^2	10^3	10^4
μ_o	2.35	3.50	4.70	5.55

Hence, the term $\left(\frac{p}{p_0}\right)^{\mu_0}$ which is associated with the enthalpy drop provides an effective cutoff for the log integral and the major contribution develops in the range where Eq. (56) is accurate. Similarly, one may approximate

$$\int_{\zeta_0}^{\zeta} \left(\frac{p}{p_0}\right)^{\mu_0} \exp\left(\delta_0 \int_{\zeta_0}^{\zeta} \frac{p}{p_0}\, d\zeta\right) d\zeta \qquad \text{by}$$

$$\int_{\zeta_0}^{\zeta} \exp\left[\delta_0 \int_{\zeta_0}^{\zeta} \frac{p}{p_0}\, d\zeta - \mu_0\left(1 - \frac{p}{p_0}\right)\right] d\zeta$$

and, upon substitution of Eq. (56), one finds

$$\int_{\zeta_0}^{\zeta} \left(\frac{p}{p_0}\right)^{\mu_0} \exp\left(\delta \int_{\zeta_0}^{\zeta} \frac{p}{p_0}\, d\zeta\right) d\zeta$$

$$\approx \frac{e^{\bar{\delta}_0 \bar{b}^2}}{2\bar{A}} \sqrt{\frac{\pi}{\delta_0}} \left\{ \operatorname{erf}\left[\bar{A}(\zeta - \zeta_0) + \bar{b}\right] \sqrt{\bar{\delta}_0} - \operatorname{erf} \bar{b} \sqrt{\bar{\delta}_0} \right\} \tag{57}$$

with

$$\bar{\delta}_0 = \frac{\delta_0}{2\bar{A}} \quad , \quad \bar{b} = \frac{\mu_0}{2\bar{\delta}_0} - 1 \tag{58}$$

The parameter $\bar{\delta}_0$ expresses the need for a higher recombination rate at the turning point to offset a larger pressure drop.

The first step is to evaluate the effect of enthalpy drop for zero recombination. The solution is defined by Eq. (55) into which Eq. (56) has been introduced. The final frozen level is given by

$$\alpha_f\left(\zeta_{max}(\xi)\,;\beta_0 = 0\right) = \alpha_0 + (4+\alpha_0) T_0'^2 \log\left[1 + \frac{\lambda_0}{(\mu_0+1)\bar{A}}\right] \tag{59}$$

The results are shown as the dashed curves in Fig. 13. The full curves represent the exact solution of Section 3.3 (for $\mu_o = \beta_o = 0$). Since the exponential approximation is accurate for $\mu_o = 0$, the comparison displays the effect of enthalpy drop. Because $(4 + \alpha_o)\, T_o'^2$ is small and of the weak logarithmic dependence, the effect of enthalpy drop is small. It is most marked for high values of $\bar{\Lambda}$. The trend is to decrease $\alpha_f(\zeta_{max})$ and make it even closer to α_o. Thus, in the present case, important departures from α_o can only be caused by recombination.

Consider now Eq. (52) for $\nu_R(\zeta_o;\eta) < 0.3$. The contribution of $\bar{\alpha}$ to α may be expressed as a sum of two terms

$$\alpha = \left(\alpha_o - \nu_R(\zeta_o)\int_{\zeta_o}^{\zeta} \frac{p}{p_o}\, d\zeta\right) + (4+\alpha_o)\, T_o'^2 \log\left[1 + \lambda_o \int_{\zeta_o}^{\zeta} \left(\frac{p}{p_o}\right)^{\mu_o} \exp\left(\delta_o \int_{\zeta_o}^{\zeta} \frac{p}{p_o}\, d\zeta\right) d\zeta\right] \tag{60}$$

The first term expresses the effect of recombination for zero dissociation rate. The second term demonstrates that the dissociation rate is enhanced by recombination. This is not surprising since, for a given pressure drop, recombination provides a mechanism for raising the temperature. A bound on the integral in the second term is obtained as follows.

$$\lambda_o \int_{\zeta_o}^{\zeta} \left(\frac{p}{p_o}\right)^{\mu_o} \exp\left(\delta_o \int_{\zeta_o}^{\zeta} \frac{p}{p_o}\, d\zeta\right) d\zeta < \lambda_o \int_{\zeta_o}^{\zeta} \left(\frac{p}{p_o}\right) \exp\left(\delta_o \int_{\zeta_o}^{\zeta} \frac{p}{p_o}\, d\zeta\right) d\zeta \tag{61}$$

$$= \frac{1}{\nu_R(\zeta_o)} \left\{\exp\left(\delta_o \int_{\zeta_o}^{\zeta} \frac{p}{p_o}\, d\zeta\right) - 1\right\}$$

At the same initial enthalpy, the normal shock solution is obtained by putting $\frac{p}{p_0} = 1$ in Eq. (50), giving

$$\alpha_{ns}(\zeta) = \left[\alpha_0 - \nu_R(\zeta_0)(\zeta - \zeta_0)\right] + (4+\alpha_0) T_0'^2 \log\left[1 + \frac{1}{\nu_R(\zeta_0)}\left\{\exp \delta_0(\zeta - \zeta_0) - 1\right\}\right] \tag{62}$$

For a given choice of Λ, Eq. (62) defines the shock solution as a function of $\eta = \bar{\Lambda}\zeta$ in the range $\alpha > \alpha_0$. The comparison of Eqs. (60), (61) and (62) suggests a new streamline coordinate, namely $\int_0^\zeta \frac{p}{p_0} d\zeta$ rather than ζ. Within the sublayer, the two streamline variables agree, since $\frac{p}{p_0}$ remains essentially constant. Beyond the sublayer but within the scaling range $\eta \leq \eta_{rec}(\eta; h_0)$, the new transformation provides a more accurate evaluation of the effect of recombination. Indeed, in this range, one expects

$$\nu_R(\zeta_0)\int_{\zeta_0}^{\zeta} \frac{p}{p_0} d\zeta \leq 0.01\,\alpha_0$$

as noted in Section 2.1; since $(4 + \alpha_0) T_0'^2$ is larger or equal to 0.03 in all cases of present interest ($\bar{\Lambda} > 10$, $0.4 \leq h_0 \leq 1$), one finds

$$\delta_0 \int_{\zeta_0}^{\zeta} \frac{p}{p_0} d\zeta = \frac{\nu_R(\zeta_0)}{(4+\alpha_0) T_0'^2} \int_{\zeta_0}^{\zeta} \frac{p}{p_0} d\zeta \leq \frac{\alpha_0}{3}$$

Consequently

$$\exp\left(\delta_0 \int_{\zeta_0}^{\zeta} \frac{p}{p_0} d\zeta\right) \approx 1 + \delta_0 \int_{\zeta_0}^{\zeta} \frac{p}{p_0} d\zeta$$

and the contribution of recombination to the right-hand side of Eq. (61) is

negligible. This result is all the more true of the left-hand side and it justifies the new adaptation of shock solutions to determine the range of validity of binary scaling.

The criterion for binary scaling is then expressed as

$$\bar{\Lambda}\ \zeta'_{max}(\xi) = \bar{\Lambda}\int_0^{\zeta_{max}(\xi)} \frac{\rho}{\rho_0}\, d\zeta \leq \tau_{rec}\left(\eta\,;\, h_0(\xi)\right) \tag{63}$$

In terms of the Newtonian solution, $\zeta'_{max}(\xi)$ is given by

$$\zeta'_{max}(\xi) = \frac{1}{\sin\xi\cos^2\xi}\int_{\xi}^{\vartheta_{max}(\xi)} \left(\frac{\sin 3\vartheta + \sin^3\xi}{\sin\vartheta}\right)^2 d\vartheta \tag{64}$$

which is plotted as the dashed line of Fig. 6. The recombination time $\zeta'_{max}(\xi)$ is typically 30% smaller than $\zeta_{max}(\xi)$ for $\xi > 0.3$ radians. As $\xi \longrightarrow 0$, ζ'_{max} tends to ζ_{max}, since $\frac{\rho}{\rho_0}$ tends to one. The equality sign in Eq. (63) defines $\xi = \xi_{rec}(\Lambda\ ;\ \eta)$ such that, for $\xi > \xi_{rec}$, recombination does not affect the concentration field. The following table lists the values of ξ_{rec} which are obtained for $h_\infty = 1$ ($U_\infty = 5.5$ km/sec in oxygen), $\eta = 10^{-6}$, 10^{-7}, and 10^{-8} and $\bar{\Lambda} = 10$, 10^2, 10^3, and 10^4.

TABLE 5

$\bar{\Lambda}$ \ η	10^{-6}	10^{-7}	10^{-8}
10	0.27	0.17	0.06
10^2	0.69	0.55	0.28
10^3	1.0	0.85	0.64
10^4	1.2	1.2	1.2

The results were derived by combining the data of Fig. 6 (for $\zeta'_{max}(\xi)$) and the values of $\chi_{rec}(\eta, h)$ defined in Fig. 2. Since $R_1(\chi_{rec}) = 0.3$, one finds

$$R_1(\chi_{rec}) = R_1\left[\alpha(\chi_{rec}; h); \eta\right] = \frac{1}{3} R_1\left[\alpha(\chi_{rec}; h); 3\eta\right] \quad (65)$$

and consequently

$$\alpha(\chi_{rec}; h) = \alpha_e(3\eta; h) \quad (66)$$

Equation (66) provides a convenient method for determining $\chi_{rec}(\eta; h)$ which does not require the computation of a complete normal shock solution. This method does not apply to airflows since R_1 depends then on more than one chemical concentration. For $\bar{\Lambda} > 10^2$ and $10^{-8} \leq \eta \leq 10^{-6}$, Table 5 shows that a large fraction of the flow field is affected by recombination. This result checks with Table 2 which indicates that, if $\bar{\Lambda} = 10^3$ and $\eta = 10^{-6}$, for instance, the flow is in equilibrium up to $\xi = 0.8$ ($h_\infty = 1$).

To evaluate the practical implications of the results listed in Table 5, the following numerical data will be applied

$$C = 4 \times 10^{21} \text{ cgs}, \quad U_\infty = \sqrt{2}\, v_d = 5.5 \text{ km/sec}, \quad \eta = \frac{\rho_\infty}{\rho_o}\frac{\rho_o}{\rho_d} \approx 10^{-5}\frac{\rho_\infty}{\rho_o} \quad (67)$$

where ρ_o denotes the atmospheric density at sea level. Equations (67) apply for pure oxygen ($\rho_d \approx 130$ gm/cc, $v_d = 3.9$ km/sec) and they

are based on the rate coefficient reported in Ref. 12 ($s = 2$). Thus, a body radius of 30 cms. corresponds to $\bar{\Lambda} = 2 \times 10^3$, 2×10^2 and 40 at altitudes[15] of 60 kft, 110 kft, and 160 kft, respectively, i.e. for $\eta = 10^{-6}$, 10^{-7}, and 10^{-8}, respectively. For the present value of U_∞ , the high chemical concentrations occur below $\xi = 0.8$ (see Fig. 7). Hence, at 60 kft altitude, chemical recombination controls the flow field around a pellet-sized body ($R_s \approx 3$ cms). At 110 kft altitude, $R_s = 150$ cms is required for recombination to affect the whole flow field. At 160 kft altitude, one should take $R_s = 750$ cms. For scaling purposes, the limit $\xi_{rec} \approx 0.3$ appears to be acceptable since only 10% of the mass flow giving rise to real-gas effects is then influenced by recombination. Thus, any $R_s < 3$ cms at 100 kft and < 75 cms at 160 kft allows scaling to higher altitude conditions.

CONCLUSIONS

The present report describes an analytic method for determining the chemical composition of the shock layer around a blunt body in hypersonic flow. The method is based on a correspondence between the chemical relaxation zone behind a normal shock and the reaction zone along a streamline. In both cases, the internal enthalpy of the gas remains essentially constant since Newtonian theory is applicable. Thus, the correspondence can be established by taking proper account of pressure and velocity distributions along streamlines. These distribtuions are defined by Newtonian theory. The correspondence is justified when three-body recombinations are neglected, that is, under conditions appropriate to binary scaling.

The similitude corresponding to binary scaling is discussed in detail and the range of validity of binary scaling is determined. By means of the above correspondence, the problem is reduced to binary scaling of normal shock solutions which is readily analyzed. The structure of the reaction zone along a streamline is investigated and a simple criterion is obtained for the concentration level at which freezing occurs. The accuracy of this criterion is ascertained by comparison with more complex analytic solutions which account for the small enthalpy drop along Newtonian streamlines. A general analytic solution including three-body recombinations is also presented.

The results show that binary scaling constitutes a useful tool for the interpretation of experimental data. For instance, the nonequilibrium flow field of a pellet-size body at 100 kft altitude and 16 kft/sec flight speed can be satisfactorily scaled to higher altitudes. In general, binary scaling allows a reliable simplification of experimental studies in modern high-enthalpy facilities.

REFERENCES

1. Gibson, W.E., Dissociation Scaling for Nonequilibrium Blunt-Nose Flows, AEDC-TDR-62-25. American Rocket Society Journal, Vol. 32, No. 2, p. 285, February 1962.

2. Hall, J.G., Eschenroeder, A.Q., and Marrone, P.V., Inviscid Hypersonic Airflows with Coupled Chemical Reactions. Paper presented at IAS 30th Annual Meeting, New York, January 1962. IAS Paper No. 62-67.

3. Gibson, W.E., and Moore, F.K., Acoustic Propagation in a Diatomic Gas Subject to Thermal or Chemical Relaxation. CAL Report HF-1056-A-2, December 1958.

4. Vincenti, W.G., Nonequilibrium Flow Over a Wavy Wall, J. Fluid Mech., Vol. 6, Part 4, p. 481-496, November 1959.

5. Freeman, N.C., Dynamics of a Dissociating Gas, III. Non-equilibrium Theory. North Atlantic Treaty Organization, AGARD Report 133.

6. Lighthill, M.J., Dynamics of a Dissociating Gas, Part I. Equilibrium Flow. J. Fluid Mech., Vol. 2, Part 1, p. 1-32, January 1957.

7. Gibson, W.E. and Marrone, P.V., A Similitude for Nonequilibrium Phenomena in Hypersonic Flight. Paper presented at AGARD Meeting on High Temperature Aspects of Hypersonic Fluid Dynamics, Brussels, Belgium, April 1962.

8. Sedov, L. I., Michailova, M. P., and Chernyi, G. G., On the Influence of Viscosity and Heat Conduction on the Gas Flow Behind a Strong Shock Wave. Vestnik Moskovskovo Universiteta, No. 3, 1953, p. 95.

9. Hayes, W. D. and Probstein, R. F., Viscous Hypersonic Similitude, J. A. S., Vol. 26, No. 12, p. 815, December 1959.

10. Cheng, H. K., Similitude of Hypersonic Real-Gas Flows Over Slender Bodies with Blunted Noses. J. A. S., Vol. 26, No. 9, p. 575, September 1959.

11. Taylor, G. I., The Formation of a Blast Wave by a Very Intense Explosion, Part I. Theoretical Discussion. Proc. Roy. Soc. (A) Vol. 201, No. 1065, p. 159-186, March 1950.

12. Byron, S. R., Measurement of the Rate of Dissociation of Oxygen, J. Chem. Phys., Vol. 30, p. 1380-1392, 1959.

13. Freeman, N. C., On the Theory of Hypersonic Flow Past Plane and Axially Symmetric Bluff Bodies. J. Fluid Mech., Vol. 1, p. 366, October 1956.

14. Freeman, N. C., On a Singular Point in the Newtonian Theory of Hypersonic Flow, J. Fluid Mech., Vol. 8, Part 1, p. 109-122, 1960.

15. Wittliff, Charles E. and Curtis, James T., Normal Shock Wave Parameters in Equilibrium Air. CAL Report CAL-111, November 1961.

16. Feldman, S., Hypersonic Gas Dynamic Charts for Equilibrium Air, AVCO Research Report 40, January 1957.

17. Logan, J.G., Jr., and Treanor, C.E., Polytropic Exponents for Air at High Temperatures. J.A.S., Vol. 24, No. 6, p. 467, June 1957.

18. Eschenroeder, Alan Q., Boyer, Donald W., and Hall, J. Gordon, Nonequilibrium Expansions of Air with Coupled Chemical Reactions, Phys. Fluids, Vol. 5, No. 5, May 1962.

19. Bloom, M.H. and Steiger, M.H., Inviscid Flow with Nonequilibrium Molecular Dissociation for Pressure Distributions Encountered in Hypersonic Flight. J.A.S., Vol. 26, No. 11, pp. 821-835, November 1960.

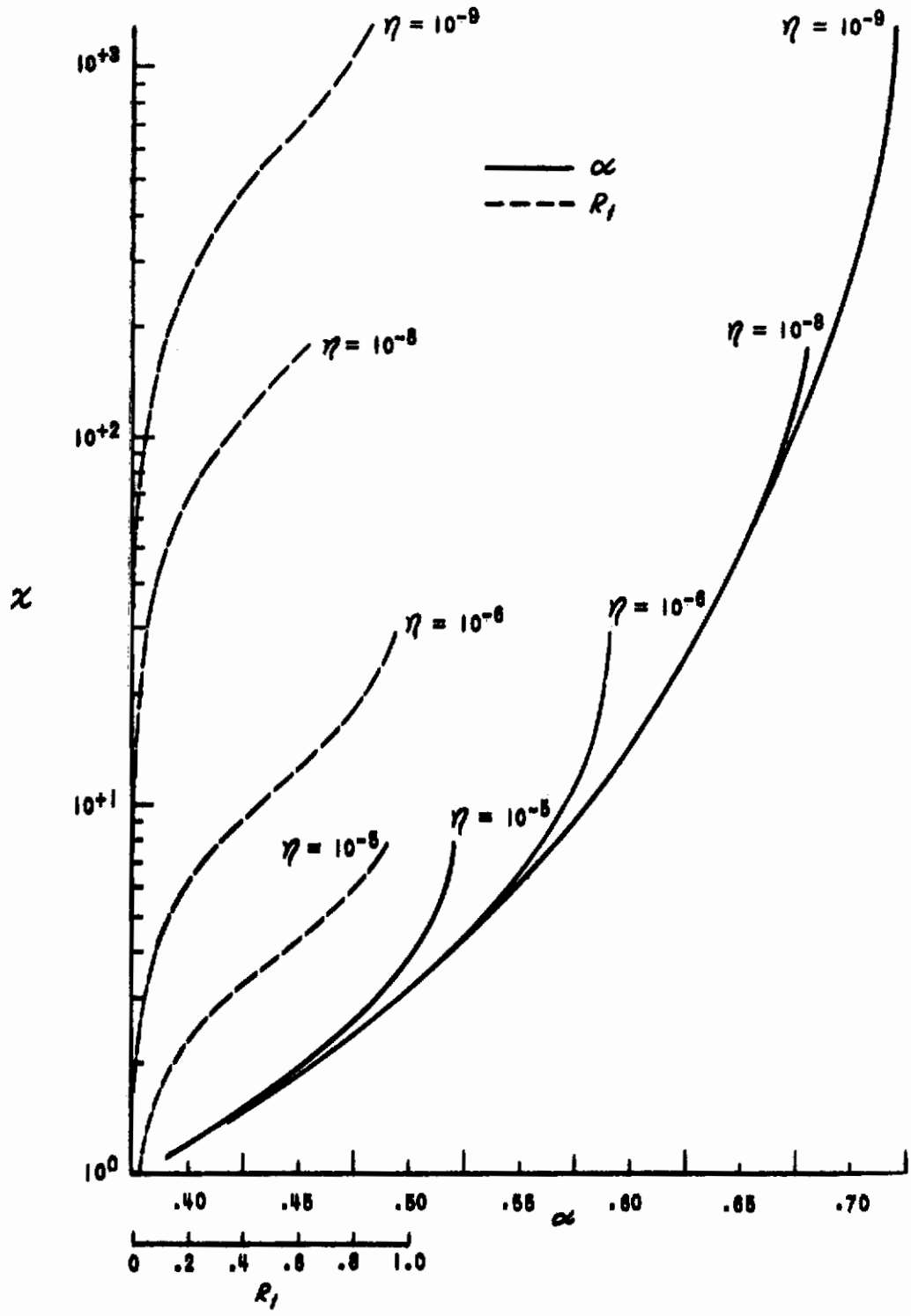

Figure 1 NORMAL SHOCK SOLUTIONS FOR A LIGHTHILL GAS

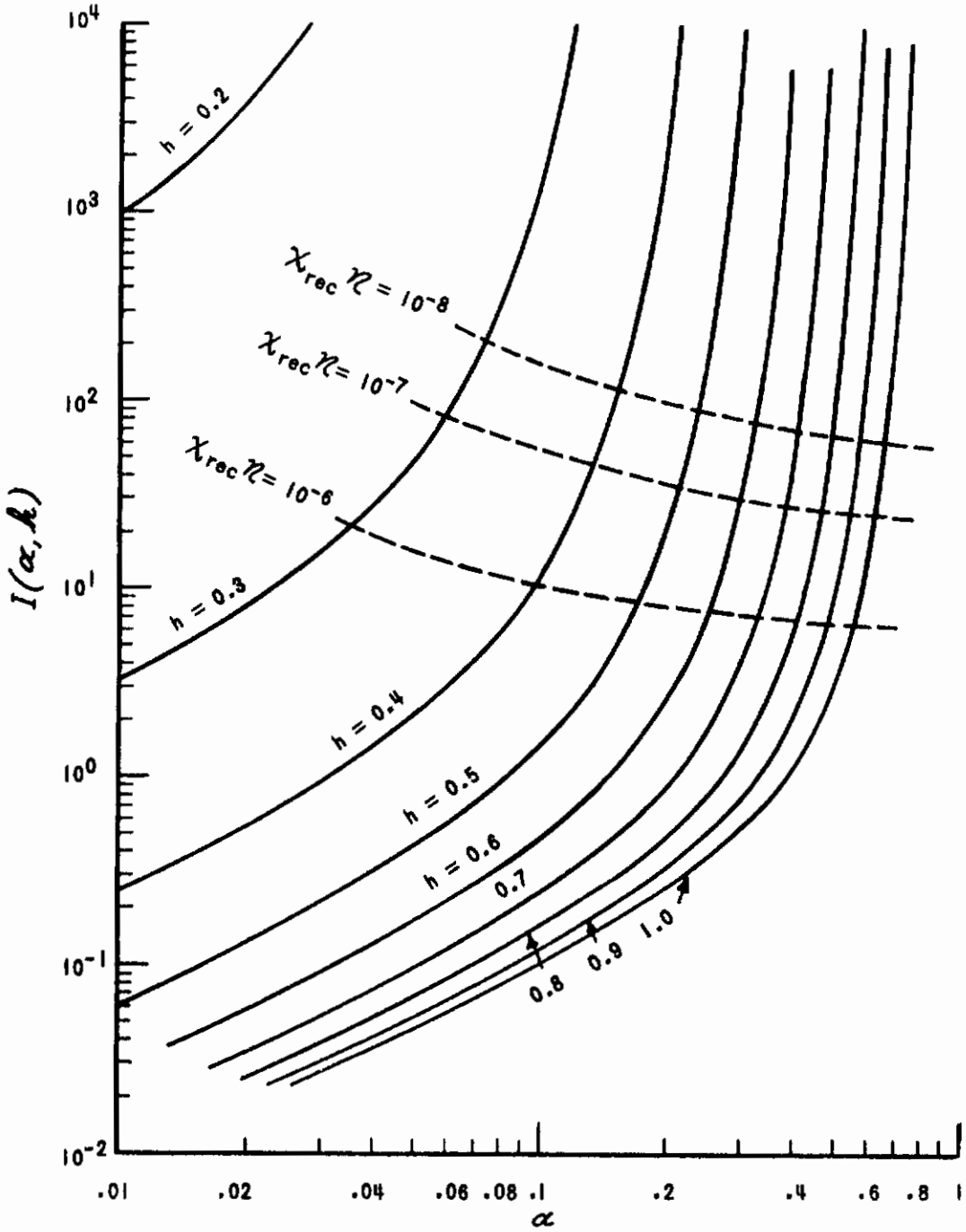

Figure 2 THE DISSOCIATION INTEGRAL I (α; h) FOR $s = 2$

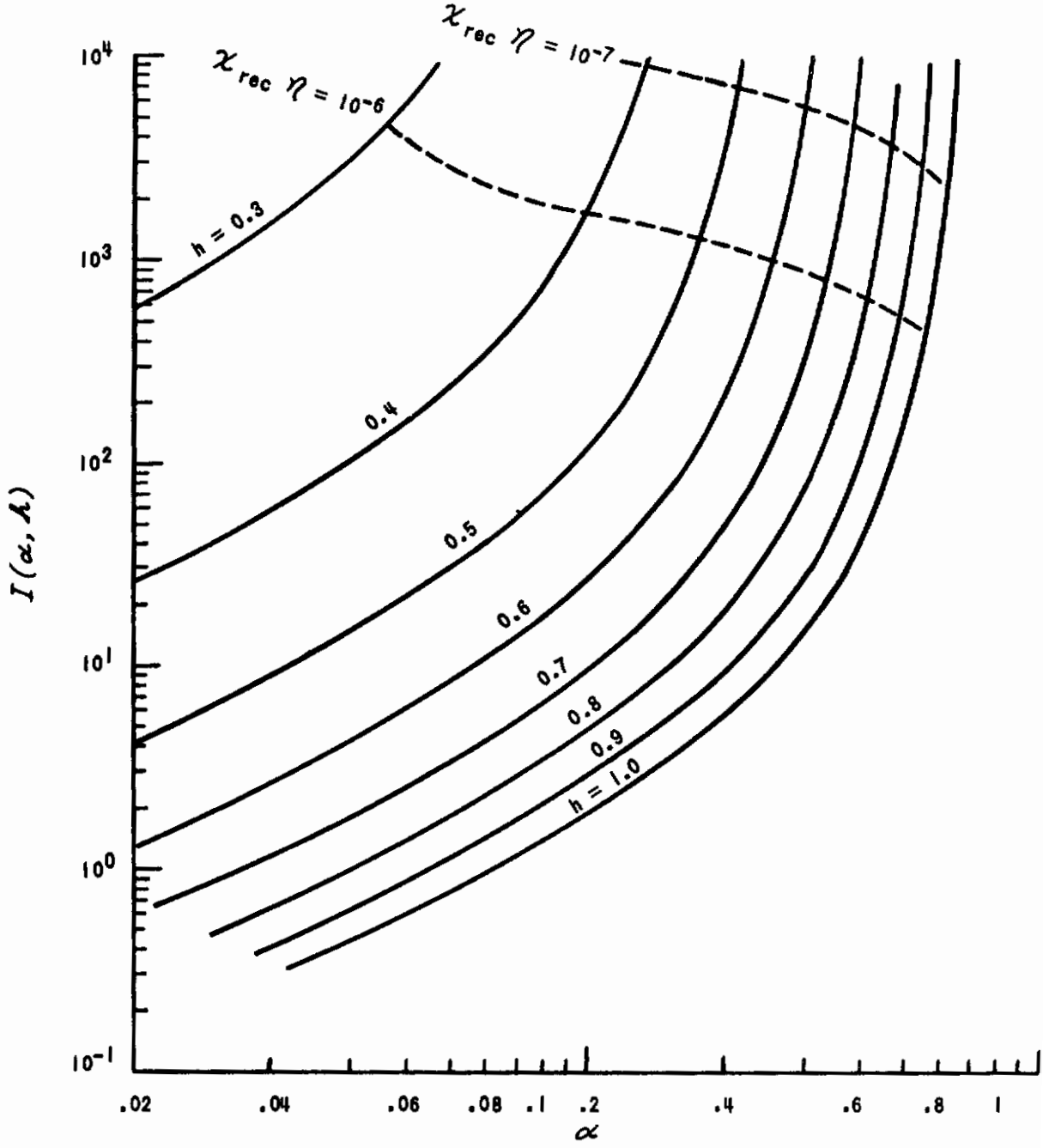

Figure 3 THE DISSOCIATION INTEGRAL I $(\alpha; h)$ FOR $s = 0$

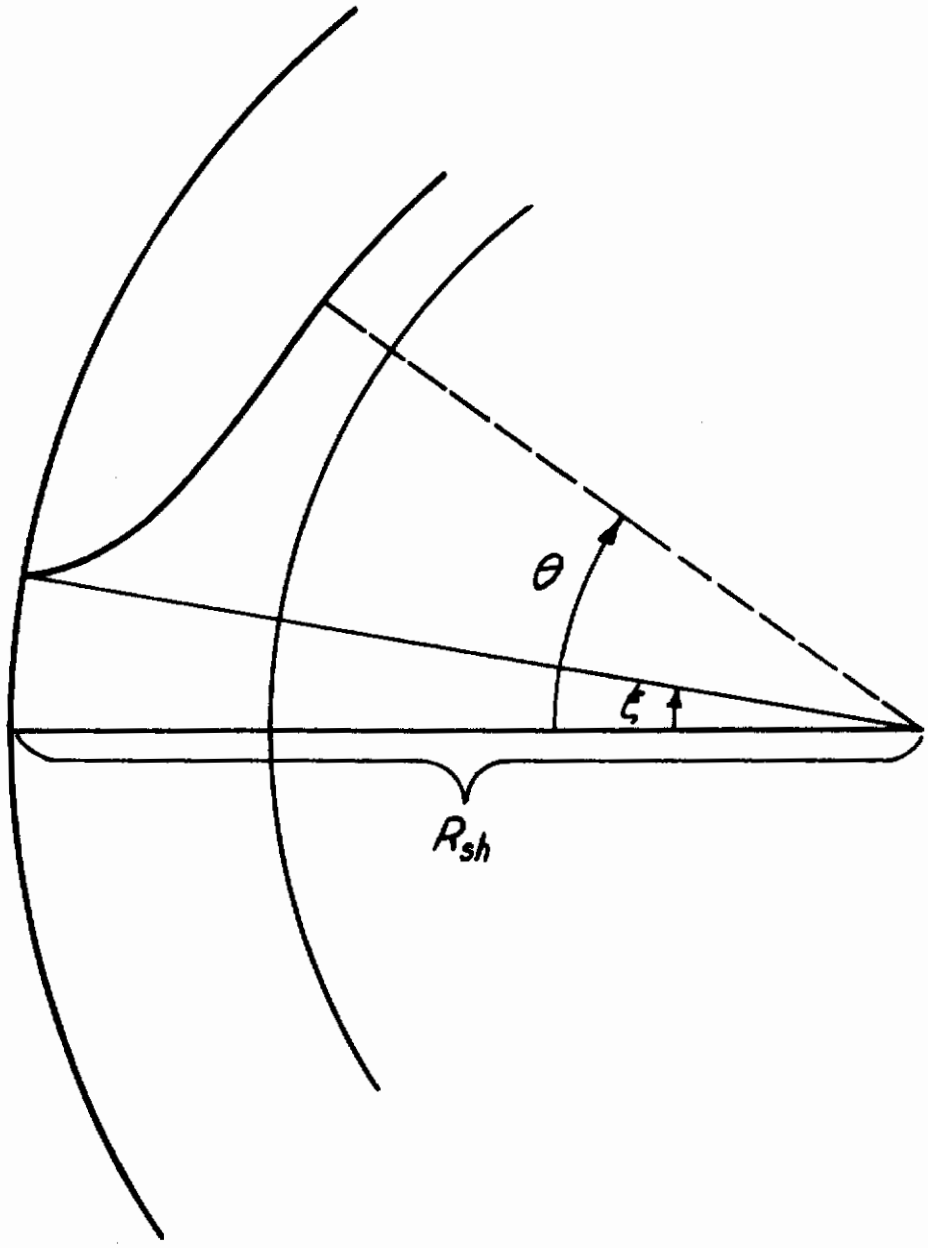

Figure 4 GEOMETRY OF SPHERICAL SHOCK

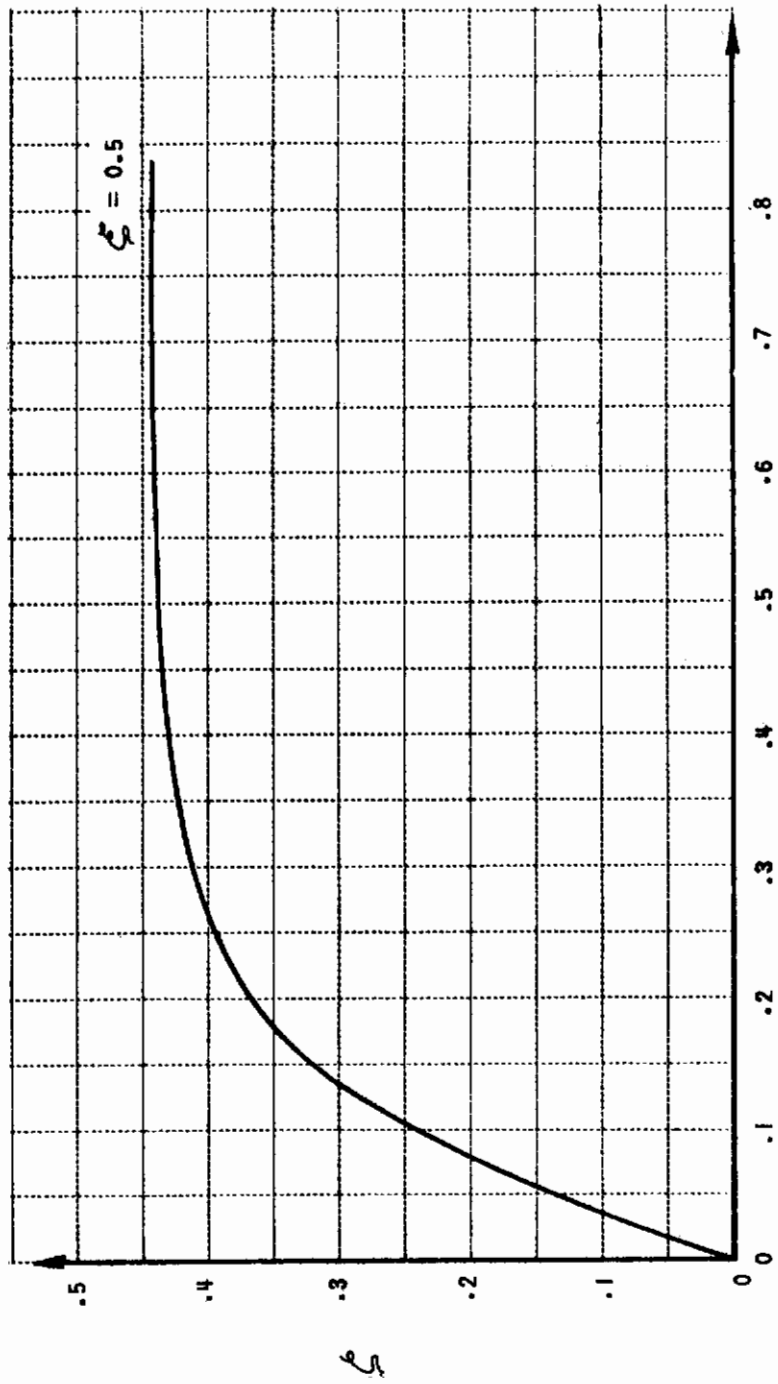

Figure 5 TYPICAL VARIATION OF $\zeta(\nu;\xi)$

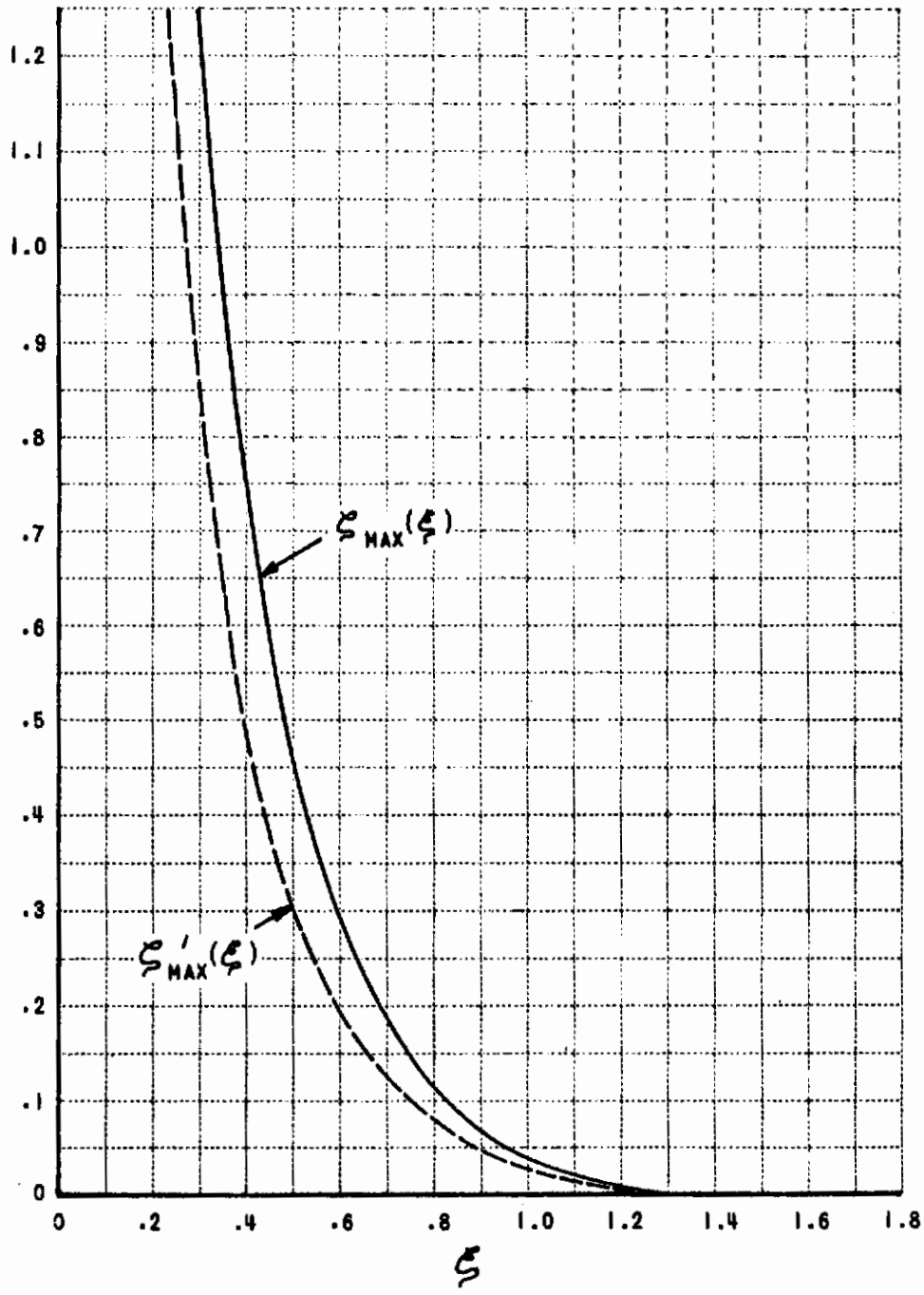

Figure 6 THE FUNCTIONS $\zeta_{MAX}(\xi)$ AND $\zeta'_{MAX}(\xi)$

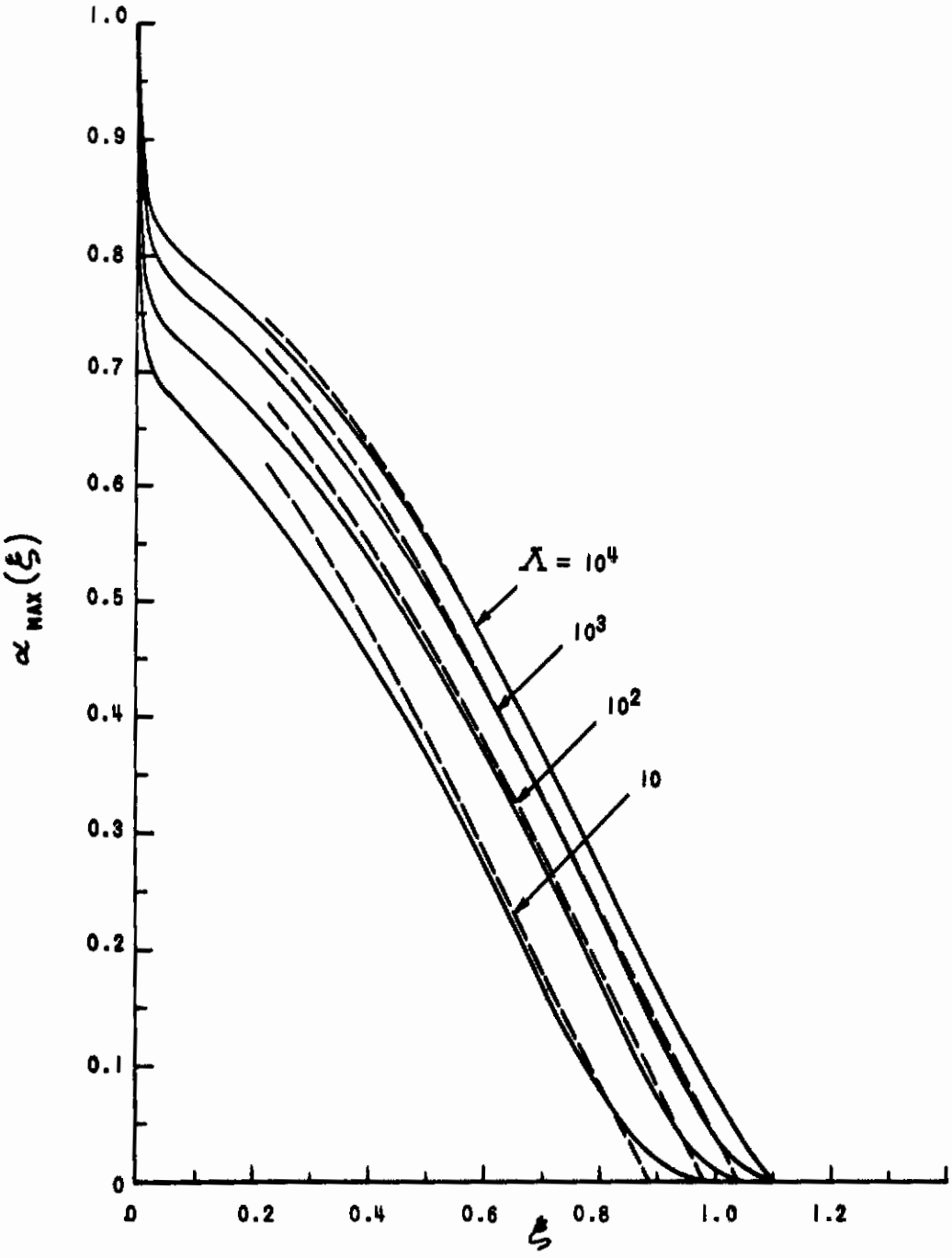

Figure 7 PROFILES OF $\alpha_{MAX}(\xi)$ FOR ZERO RECOMBINATION

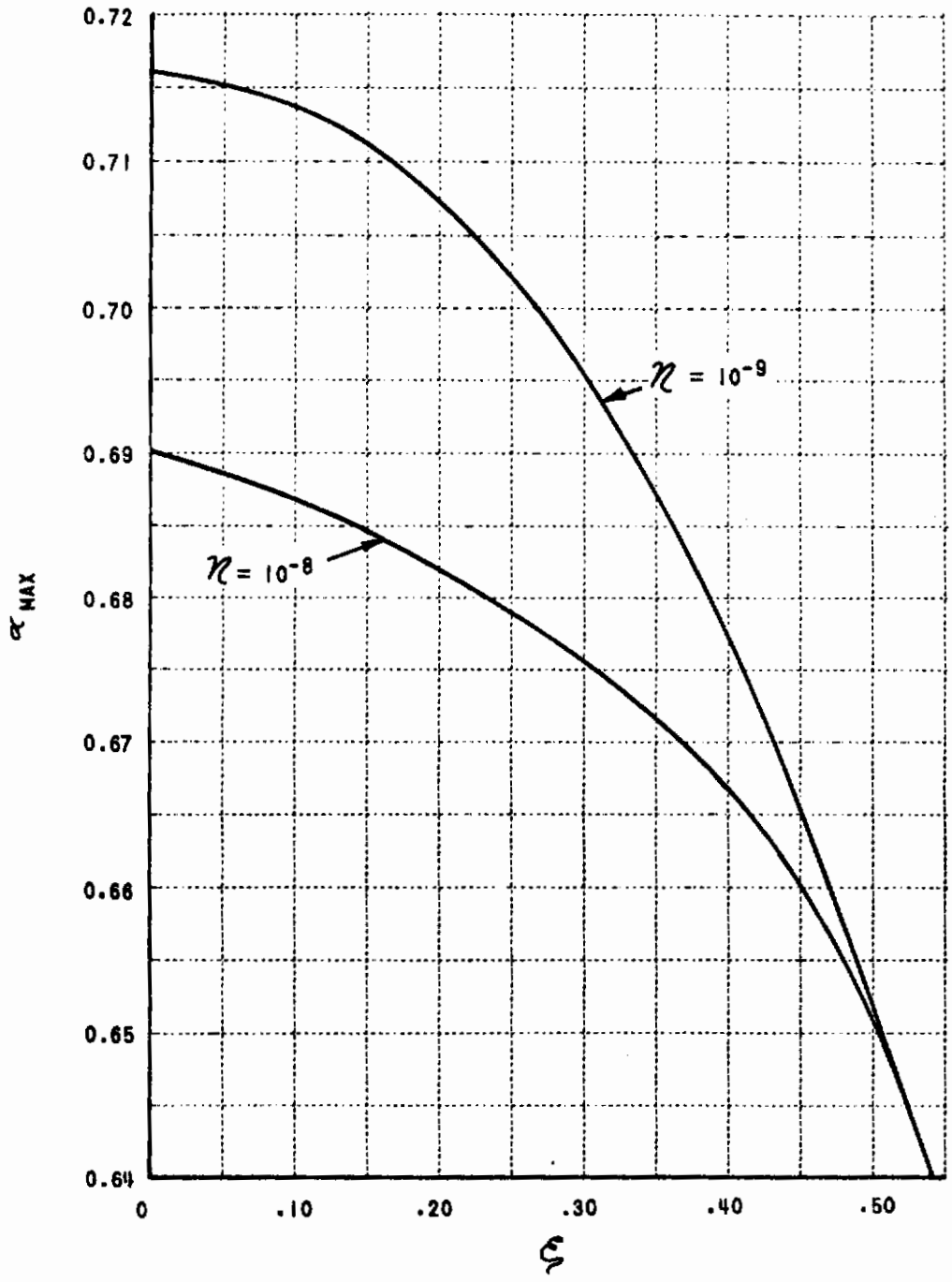

Figure 8 EFFECT OF RECOMBINATION NEAR THE BODY

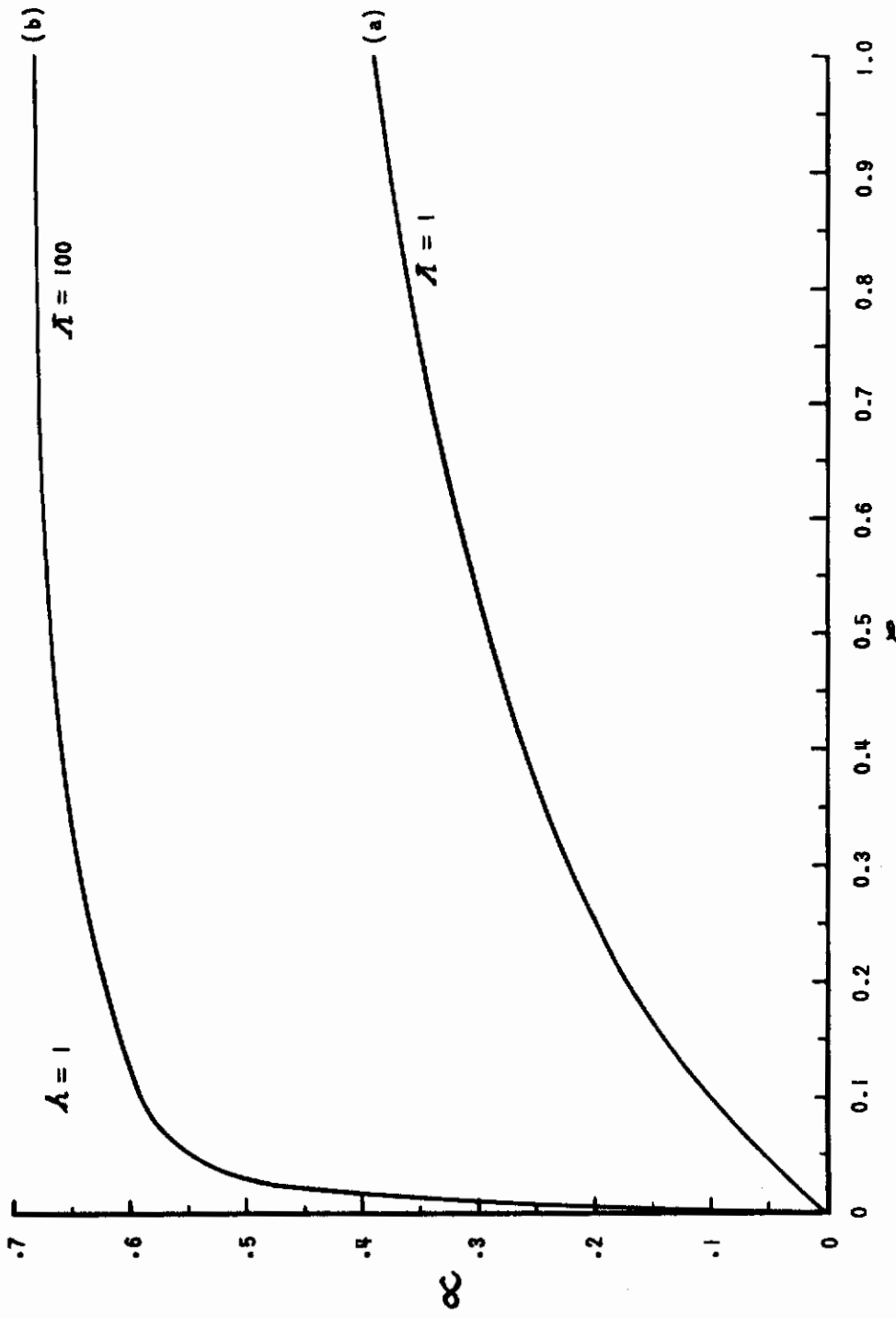

Figure 9 TYPICAL CONCENTRATION PROFILES

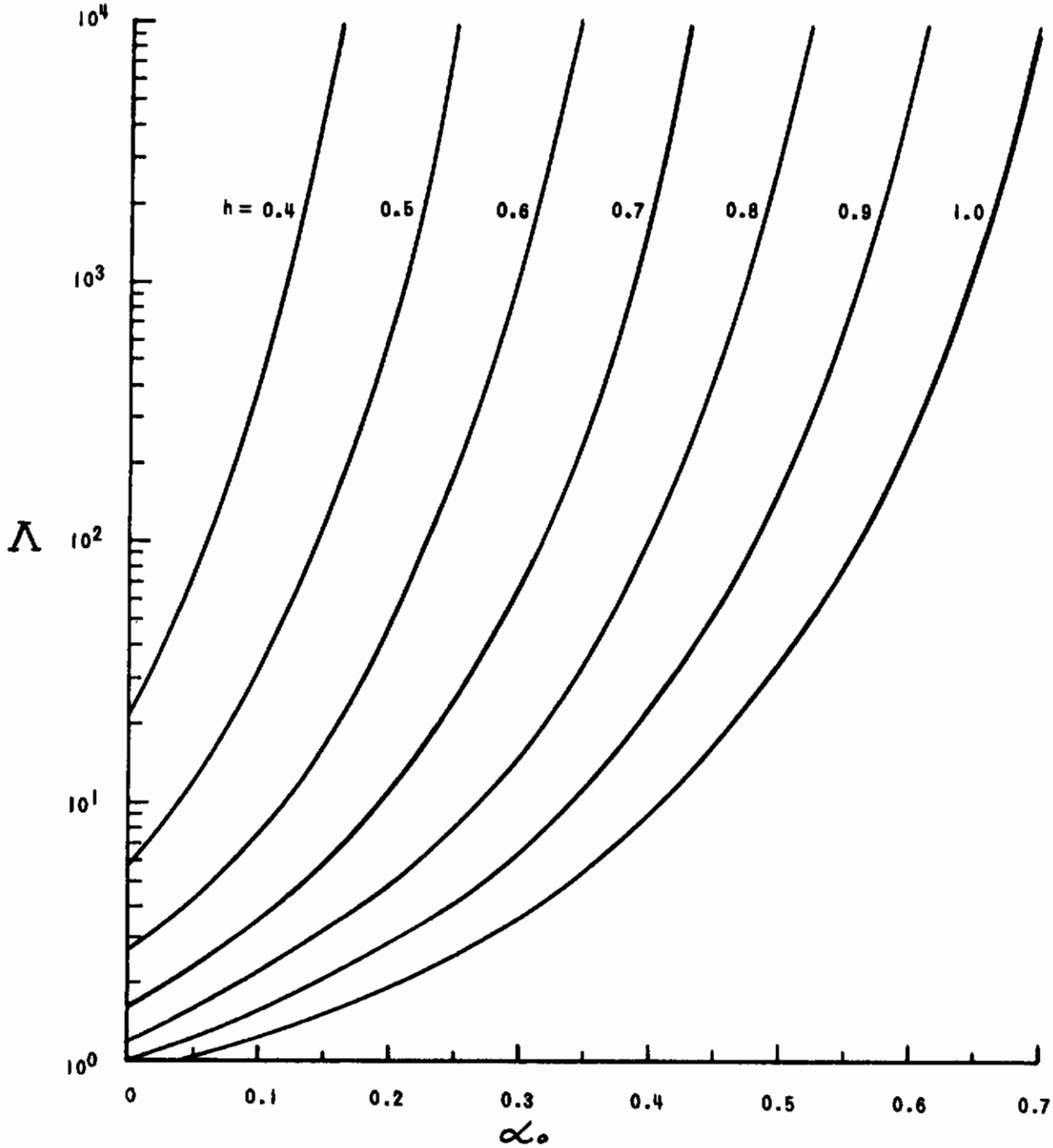

Figure 10 THE FUNCTION α_o $(\bar{\Lambda}; h)$

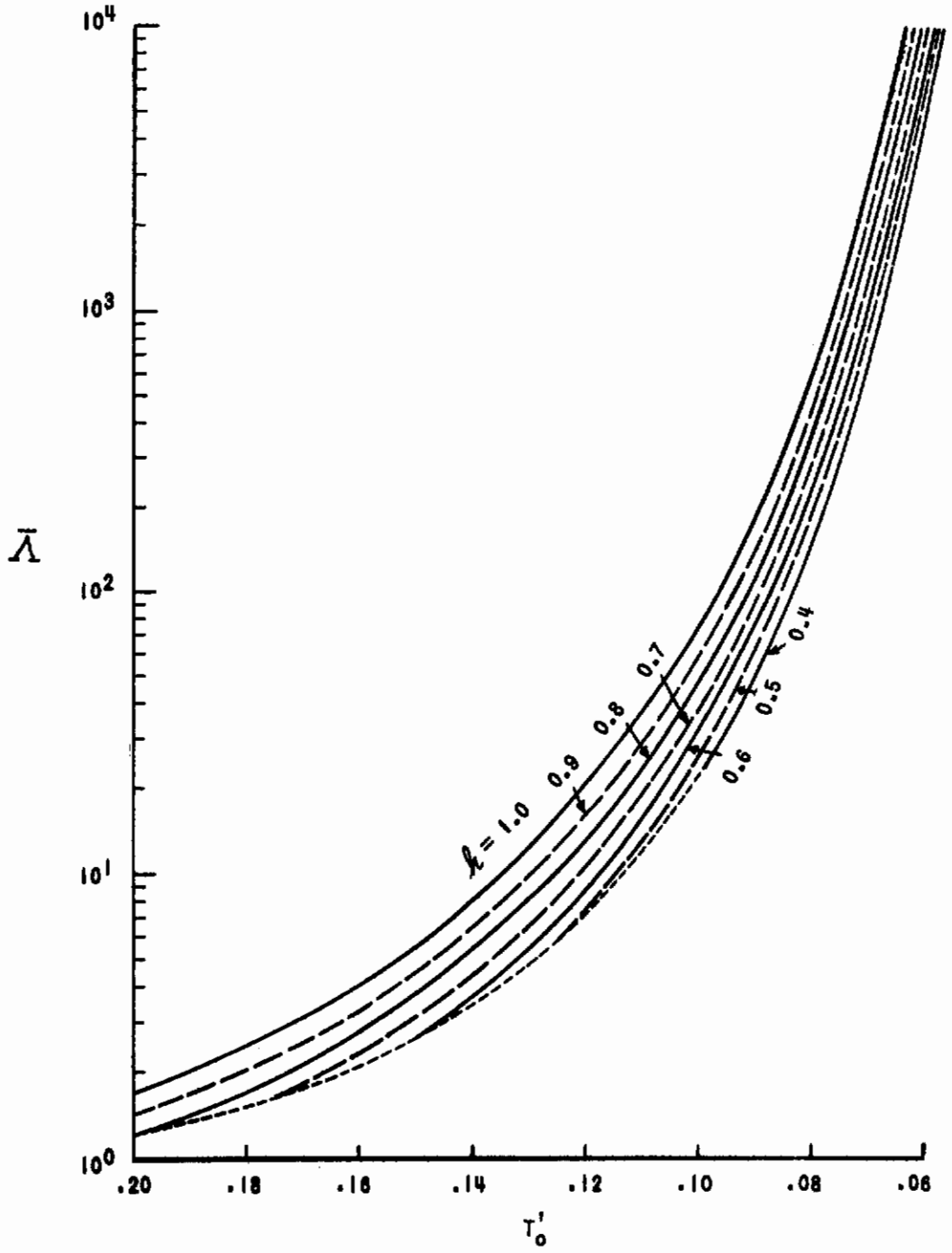

Figure 11 THE FUNCTION $T_o'(\bar{\Lambda}; k)$

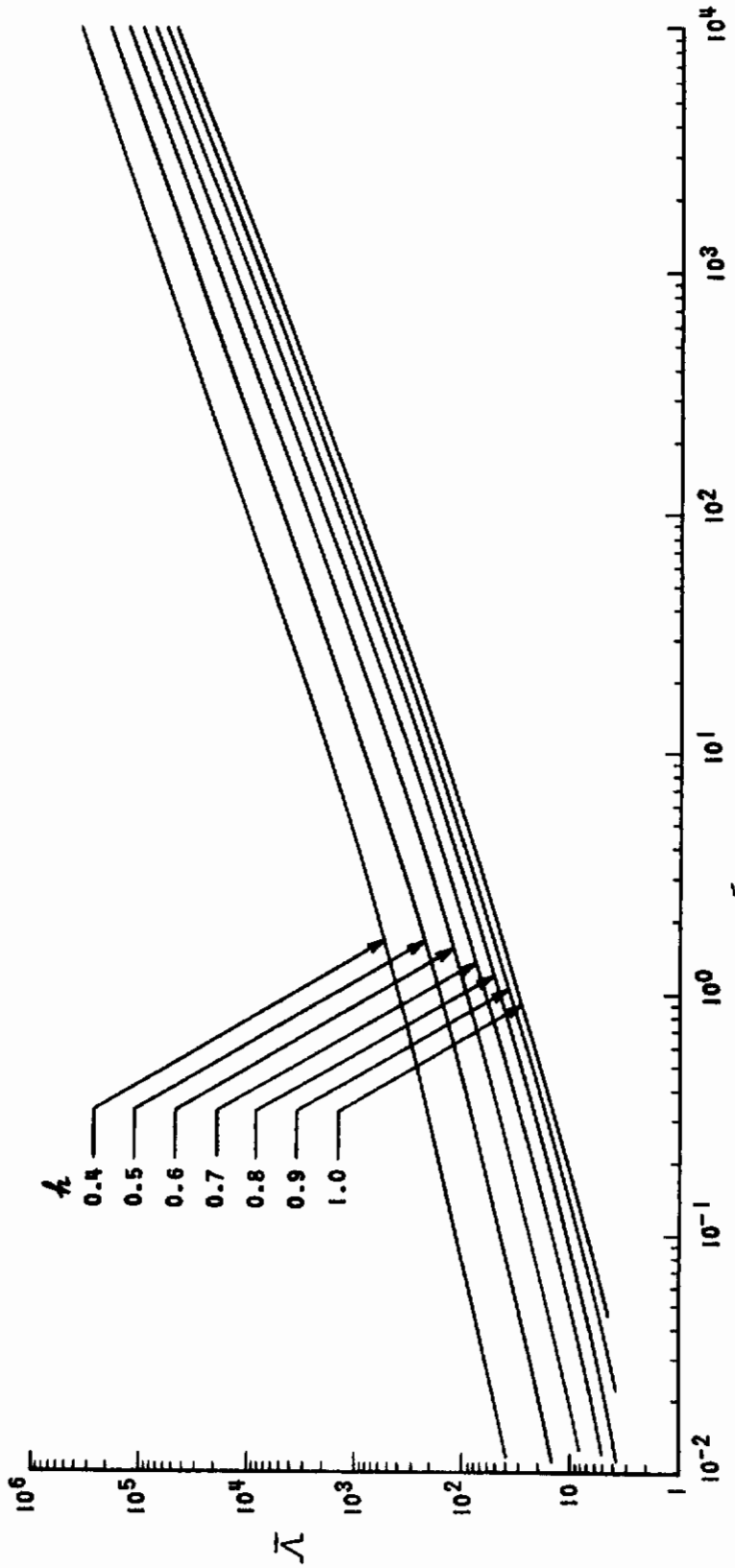

Figure 12 THE RECOMBINATION RATE $\frac{10^{-5} n_R(\xi_0)}{\eta}$

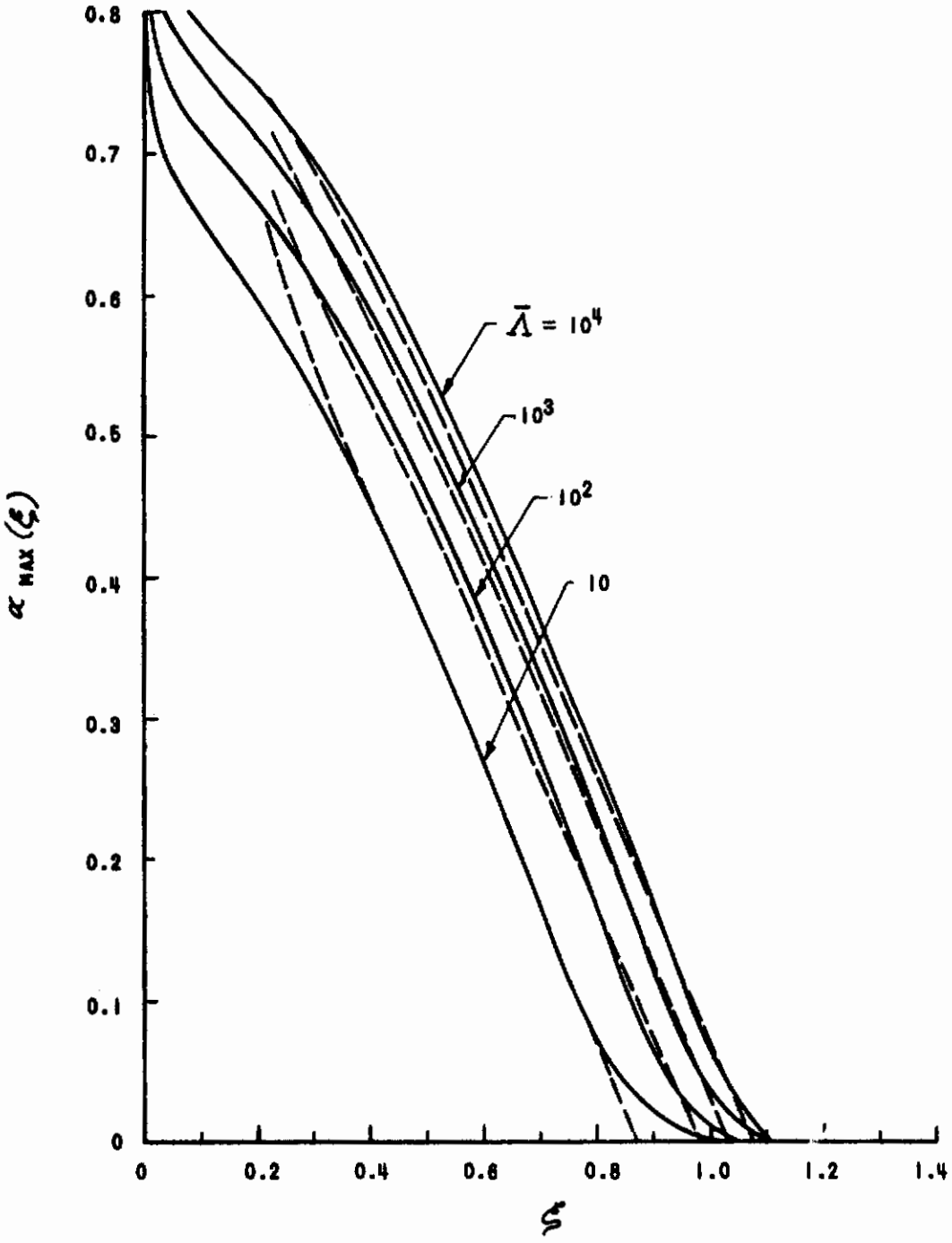

Figure 13 EFFECT OF ENTHALPY DROP FOR ZERO RECOMBINATION